Annu. Rev. Nucl. Part. Sci. 1993. 43:585–633

QCD TESTS IN PROTON-ANTIPROTON COLLISIONS

John E. Huth

Dept. of Physics, Lyman Laboratory, Harvard University, Cambridge, Massachusetts 02138, USA

Michelangelo L. Mangano

Istituto Nazionale di Fisica Nucleare, Scuola Normale Superiore and Dipartimento di Fisica dell'Universita', Pisa, Italy

KEY WORDS: jets, hadrons, gluons, quarks, photons, structure functions

CONTENTS

0163-8998/93/1201-0585$2.00

1. INTRODUCTION

Quantum Chromodynamics (QCD) is regarded as the best, if not the only, viable theory of the strong interactions (1, 2). Recent theoretical and experimental developments have significantly increased our ability to perform quantitative tests (3) and have deepened our understanding of hadronic interactions. This is particularly true for higher energy processes, where the decreasing value of the coupling constant $\alpha_s(\mu)$ allows reliable results from a perturbative expansion (4–13). In addition, the nonperturbative transition from the fundamental objects in the theory (quarks and gluons) to observed particles (hadrons) has a smaller influence on measured quantities. At the energies now accessible, one is expected to be far away both from the long-distance regime where perturbation theory breaks down and from the ultra-short-distance regime where one might witness the onset of new dynamics. This, however, does not excuse one from vigilance for significant deviations from perturbative predictions.

Tests of QCD in hadron-hadron collisions display a parallel development in both theory and experiment. The earliest measurements of high p_t hadron production at the ISR belied the then hidden partonic component of the proton. The observations of jets and early tests of QCD at the $S\bar{p}pS$ (16) were largely qualitative, yet they demonstrated the predictive power of the theory at leading order in perturbation theory. Currently we are entering a period in which the emphasis is being placed on measurement precision. From an experimental standpoint, this emphasis requires making measurements with high statistics and small systematic uncertainties. From a theoretical standpoint, it means calculating quantities at successively higher orders in perturbation theory, and using constraints from a number of sources (for example, parton distribution functions) to pin down predictions. In the interplay between theory and experiment, there must be a coherent view of how quantities are defined (e.g. what precisely is a "jet"?) in order to arrive at definitive tests.

Recent studies with high statistics of hadronic decays of the Z^0 from e^+e^- production have yielded impressive new confirmations of the theory (14). QCD tests in $p\bar{p}$ collisions are not as direct as those in e^+e^- owing partly to the complications associated with partons in the initial state and with the beam fragments (the so-called underlying event). Accompanying this complexity, however, is a richness that allows one to attack a given problem in a number of complementary ways. For example, on the one hand, knowledge of the partonic density as a function of the proton momentum fraction introduces uncertainties

in the predictive power of the theory. On the other hand, the same feature allows one to obtain data spanning a wide range of center-of-mass energies in the parton-parton frame for a fixed set of beam conditions. The variety and diversity of hard processes accessible in hadronic collisions, together with the enormous cross sections and energy reach, provide us with a multitude of phenomena inaccessible to current e^+e^- experiments (15–20).

A major ingredient for the prediction of cross sections in $p\bar{p}$ collisions is the distribution of partons inside the proton (21, 22). Recently there has been significant progress in theory and experiment, leading to expanded measurements of parton distribution functions. Concurrently, next-to-leading order (NLO) perturbative calculations have been performed for most interesting processes. As a result we have collected a substantial body of evidence demonstrating that QCD properly describes this physics both qualitatively and quantitatively. However, some outstanding questions remain to be resolved. The aim of this review is to present the evidence in a critical way, pointing out where theoretical and experimental improvements are expected or desired and where one can rely on QCD to extract new information.

We review the last analyses from the CERN Collider experiments (UA1 and UA2), which completed their operations in 1991, along with data from the Collider Detector at Fermilab (CDF) dating mostly from the 1988–1989 running period of the Fermilab Tevatron. A new cycle of data-taking started in the summer of 1992 at the Fermilab Collider, with the presence of a new experiment, D0. Several of the results presented here are still on their way to press and are available only in preprint form. We felt it necessary to include them because they often add important new contributions to the overall picture. We regret that the analyses from the latest set of data collected since summer 1992 are still premature to appear in this review, and we look forward to their completion for the important implications they will have on the study of QCD in hadronic collisions.

2. QCD IN HADRONIC COLLISIONS

One of the fundamental properties of QCD is the shrinking of the coupling constant as the energy of the interaction grows (asymptotic freedom). This implies that perturbative techniques can be used to study high energy hadronic phenomena. In spite of this, we cannot fully rely on perturbation theory because the fundamental particles whose interactions become weak at high energy are deeply bound inside the hadrons we use as beams, as targets, or as observables. The solution

is given by factorization theorems (11, 12), whereby cross sections can be expressed as the product of factors, each one involving phenomena at different energy scales.

In hadronic collisions, the separation of the initial-state evolution from the hard perturbative interaction can be represented, for a generic inclusive process $A + B \to C + X$, as

$$\sigma_{A+B\to C+X} = \sum_{ij} \int dx_1\, dx_2\, f_i^A(x_1, \mu_F) f_j^B(x_2, \mu_F) \hat{\sigma}_{ij\to C}[\hat{s}, \mu_F, \mu_R, \alpha_s(\mu_R)], \quad 1.$$

with $\hat{s} = x_1 x_2 s$. The indices i and j represent any pair of partons (quarks or gluons) contributing to the process, $f_i^A(x, \mu_F)$ represents the number density of partons of type i carrying a fraction x of the momentum of the parent hadron A, and $\hat{\sigma}$ is the cross section for the elementary hard process, calculable in perturbation theory.[1] Furthermore, the parton distribution functions (PDFs) $f(x, \mu_F)$ are independent of the specific reaction. The universality of PDFs is a key property; they are not calculated from first principles because they contain nonperturbative information, but they can be extracted from one process and applied to predict rates for another one.

The scale μ_R introduced above is the scale at which the ultraviolet singularities of the theory are subtracted ("renormalization prescription"), determining the "running" of $\alpha_s(\mu_R)$. The energy scale μ_F represents the freedom given by the factorization theorem to absorb as much or as little of the radiation from the evolution of the initial-state parton into the PDF, including the rest in $\hat{\sigma}$ ("factorization prescription").

The final result should not depend on the choice of μ_F and μ_R. This will be true if we evaluate $\hat{\sigma}$, $\alpha_s(\mu_R)$, and $f(x, \mu_F)$ exactly. Any fixed-order perturbative approximation will leave a residual dependence on μ_F and μ_R. This dependence is logarithmic, and the sensitivity of a fixed-order cross section to variations of $\mu_{F,R}$ is usually taken as an estimate of the importance of neglected higher order terms. Since the two scales have different origins, they do not have to be the same. Nevertheless it is customary to take them equal and of the order of the energy scale of the hard subprocess, to avoid the appearance of logarithms of large ratios in the perturbative expansion and to minimize

[1] If C were a specific hadron, an independent factorization theorem for fragmentation would apply. The cross section $\hat{\sigma}$ will then be the convolution of a purely partonic process with a fragmentation function describing the transition of a final-state parton into C.

the effect of higher order terms. The invariance of the results under changes of μ_F allows one to formulate an equation [the Altarelli-Parisi equation (23)] that "evolves" the PDF from one scale μ_F to another. With this equation, measurements of the PDF carried out at relatively low values of μ in deep inelastic scattering experiments can be used to extrapolate the values of parton densities to the values of μ found in hard hadronic collisions.

The cross sections derived at leading order have large uncertainties associated with the choice of μ, since the matrix elements at this order do not contain any initial-state radiative process and are thus independent of μ_F. A dependence on μ_F appears inside $\hat{\sigma}$ only at the next order in perturbation theory (via the subtraction of the initial-state collinear singularities) and a partial cancellation between $f(x,\mu_F)$ and $\hat{\sigma}(\mu_F)$ takes place. It is therefore important to have available at least the NLO matrix elements to carry out quantitative tests of QCD. In spite of the technical difficulties, the calculation of most of the interesting processes has been completed today at NLO accuracy, and new techniques are being developed to enable the calculation of yet higher order corrections (13, 24, 25).

Likewise, analyses of the PDFs have been carried out in recent years with similar precision, providing the necessary elements for consistent NLO calculations (26–35). We refer the reader to earlier reviews in this series for discussions of PDF measurements and parameterizations (21, 22). Here we limit ourselves to pointing out the existence of recent data extending the measurements of $F_{2,3}(x,Q)$ down to $x = 0.008$ for Q^2 as large as 5 GeV^2 (36, 37). These data show clear discrepancies with previous extrapolations of F_2 to small x, which indicate a violation of the light flavor symmetry in the sea densities. Nevertheless the measurements confirm (37) earlier estimates of the behavior of the gluon density, whose extrapolation to small x is responsible for systematic uncertainties in the calculation of most hadronic processes. New fits to these data show that the gluon density is now under a rather solid control in the region $x > 0.01$ and $Q > 10$ GeV (34, 35) (Figure 1). This is the region of sensitivity for most QCD processes probed by current hadron colliders.

The formalism described so far only allows the calculation of inclusive quantities. These include jet distributions and correlations, or electroweak boson cross sections. The inclusive nature of the PDF by itself prevents predictions on the structure of the radiation emitted during the initial-state evolution. A more exclusive picture of the event structure is often required, both as a tool to understand the experimental systematics (calorimeter energy response, effect of particle isolation

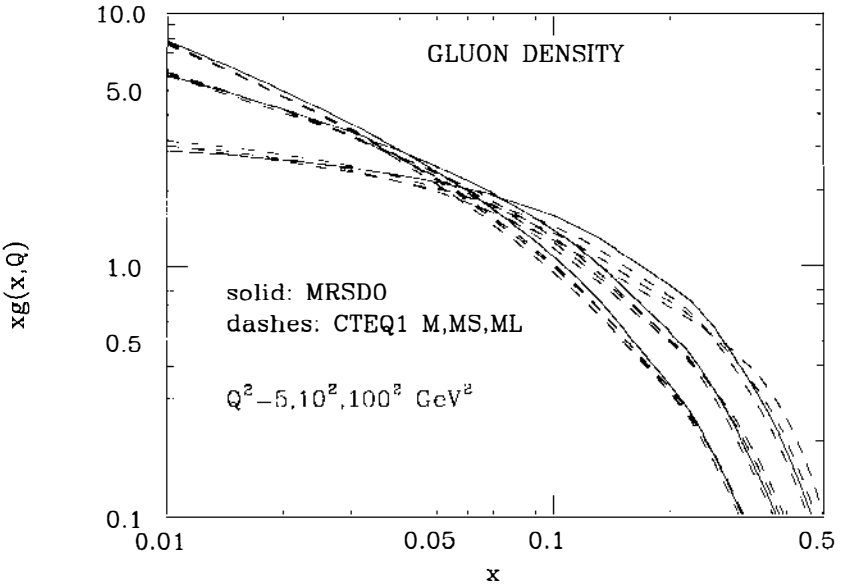

Figure 1 Gluon densities according to the most recent PDF analyses: MRSD0 (34) and various CTEQ fits (35). For $0.01 < x < 0.01$ and $Q > 10$ GeV, differences never exceed the 10% level.

requirements, etc) and as a way of probing more specific predictions of QCD (e.g. jet fragmentation properties).

To complete the description of the event structure, a complementary approach, known as shower Monte Carlo, has been developed (10). Here the partons from a hard collision evolve via gluon and quark radiation, until a small virtuality scale Q_0 is reached where $\alpha_s(Q_0)$ is large. Here confinement forces take over, hadronizing the colored partons. Descriptions of the hadron formation phase can be included (38, 39) and tuned using a reference process (e.g. jet production in e^+e^- collisions). These nonperturbative effects are believed to be universal, namely they do not depend on the hard process. The main features of the final state of different processes are thus accounted for by the QCD evolution, as the distributions of the hadrons are expected to mimic closely those of the partons they originated from (40, 41).

Such models have been implemented in several computer programs (42–48). They differ from one another in several aspects, ranging from the accuracy of the perturbative evolution to the hadronization scheme. The spectrum of the radiation is given by perturbative QCD, and in some cases (48), it includes all orders of leading and large classes of

subleading soft and collinear logarithms (9, 49). Monte Carlo programs such as PYTHIA (47) and HERWIG (48) successfully describe typical quantum mechanical effects from color interference via a simple "angular ordering" prescription, which limits the kinematical phase space available for the emission of soft gluons from colored currents (10, 40).

3. JET PRODUCTION

3.1 *Inclusive Jet Production*

The precision of QCD tests involving jets has been limited by the necessary correspondence between the final-state sprays of hadrons and the partons from a hard scattering, whose cross sections are perturbatively calculable. There have been substantial developments resulting from the higher center-of-mass energies and an improved understanding of experimental systematics. The recent calculation of jet cross sections beyond leading order in perturbation theory reduces the theoretical uncertainties greatly and predicts new quantities.

The inclusive jet cross section, $\sigma(p\bar{p} \rightarrow \text{jet} + X)$ is the most straightforward quantity to test. At leading order, $O(\alpha_s^2)$, eight diagrams contribute to the scattering and give rise to two parton final states (50). At $O(\alpha_s^2)$, the partonic cross section is directly equated to the measured jet cross sections. For a fixed $p\bar{p}$ center-of-mass energy, the inclusive cross section is a nontrivial function of two variables: η, the jet pseudorapidity ($\equiv \log \cot \theta/2$, where θ is the polar angle), and the transverse energy, E_t. As discussed below, the issue of how precisely one defines jet E_t is important to the overall consistency of the comparison between theory and experiment. For now it can be taken to be the sum of the transverse energies of discrete subunits, be they particles or calorimeter towers. The most common representation of the data is typically in terms of the differential cross section, $d\sigma/dE_t$; this is really an average of the inclusive cross section over some pseudorapidity interval in a detector:

$$\left\langle \frac{d\sigma}{dE_t} \right\rangle \equiv \frac{1}{\Delta\eta} \int_{\eta - \Delta\eta/2}^{\eta + \Delta\eta/2} \frac{d\sigma}{dE_t d\eta} d\eta. \qquad 2.$$

In some cases this is expressed as the cross section evaluated at $\eta = 0$: $(d\sigma/dE_t)|\eta = 0$, assuming that the rate is constant in η over a large enough interval. Most collider experiments report measurements in roughly the central two units of pseudorapidity.

As mentioned in Section 2, large uncertainties are associated in leading order to changes in the factorization/renormalization scale μ. For a range of $2E_t > \mu > E_t/2$, the leading order cross sections for $d\sigma/dE_t$

vary by approximately 50%. This uncertainty is roughly a constant multiplier of the cross section for different E_t's, with only a modest dependence of the shape of the cross section as a function of jet E_t.

Despite the large uncertainties, if one chooses a renormalization scale ($\mu = E_t/2$) and compares data to QCD for Tevatron ($\sqrt{s} = 1.8$ TeV) (54), Sp$\bar{p}$S ($\sqrt{s} = 630$ GeV) (51, 52), and ISR ($\sqrt{s} = 63$ GeV) (53), one finds an impressive agreement between the experimental results and the theory, with only one floating parameter. The comparison is shown in Figure 2.

The UA2 collaboration also measured the jet cross section for different pseudorapidity intervals (51). Although not shown here, the agreement is good in the central region ($|\eta| < 0.8$), but for larger values of pseudorapidity ($1.2 < |\eta| < 2.0$) agreement is marginal (51). There is no clear explanation for the discrepancy.

To calculate the cross section at next-to-leading order, one must combine graphs in which a parton is radiated with loop diagrams (Figure 3). At this order, factors of $\log(\mu)$ appear, cancelling some of the μ dependence in $\alpha_s(\mu)$ and the PDFs. The evaluation of the full NLO matrix elements was initiated by Ellis et al (55) and later completed by Ellis & Sexton in 1986 (56). A confirmation of these results using

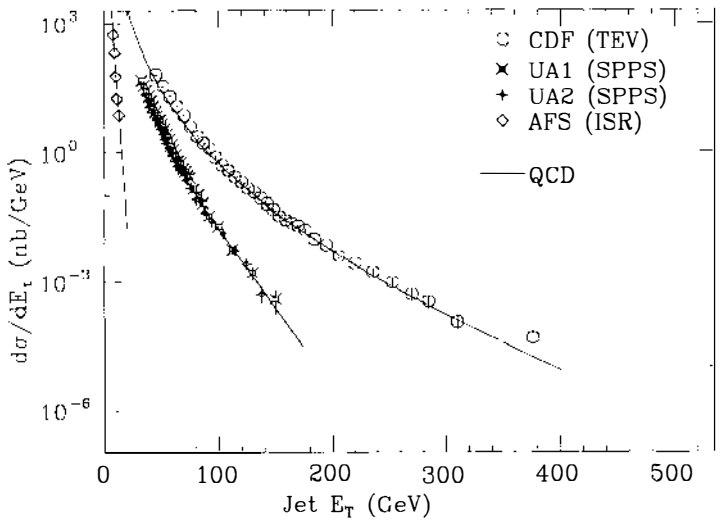

Figure 2 Comparison of the inclusive jet cross section for leading order QCD predictions with experiments at the ISR (65), Sp$\bar{p}$S (5), and Tevatron (53) colliders. Only one free parameter in the theory has been fixed (renormalization scale) in order to obtain this figure.

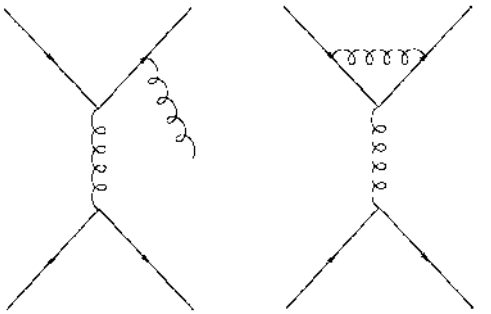

Figure 3 Examples of diagrams contributing to the jet cross section at $O(\alpha_s^3)$. Collinear and soft singularities cancel between loop and tree diagrams, after imposition of a sensible jet definition involving finite opening angles for the final-state partons.

a different approach has come recently from Bern et al (25). These works did not include an explicit calculation of the cross section. Whereas at leading order a direct correspondence is made between jet and partonic cross sections, the situation is not as straightforward at next-to-leading order. To evaluate the cross section at $O(\alpha_s^3)$ [in fact even to obtain finite results (57)], one must specify what a jet is at the partonic level. If two partons are close together, they may be merged into a single "jet." Here one speaks only of jet, as opposed to partonic cross sections at both the theoretical and the experimental levels. Ideally, the theoretical jet definition should thus be as close as possible to the experimental jet definition.

Aversa et al (58) and Ellis et al (59) used the matrix elements of Ellis & Sexton (56) to derive jet cross sections at $O(\alpha_s^3)$. Although the groups employ different computational techniques, the results are numerically identical (60). After the imposition of a jet definition (see below), the NLO cross sections show substantially smaller sensitivities to renormalization scale variations than at leading order. Over a range of renormalization scales close to the hard scattering scale ($E_t/4 < \mu < E_t$), the uncertainties in the cross section have been reduced from 50% to 10% over most of the range of accessible E_t. The inference is that the effects of still higher order contributions are rather small at $O(\alpha_s^3)$. Figure 4 shows the variation of the $O(\alpha_s^3)$ and $O(\alpha_s^2)$ cross sections with μ for 100-GeV jets. At leading order, one finds a large monotonic variation of the cross section with μ, whereas at $O(\alpha_s^3)$, the negative $\log(\mu)$ contributions from the virtual terms reduce the cross section at very small μ. Note that the sensitivity of the cross section at renormalization scales near the hard scattering scale is greatly reduced at next-to-leading order.

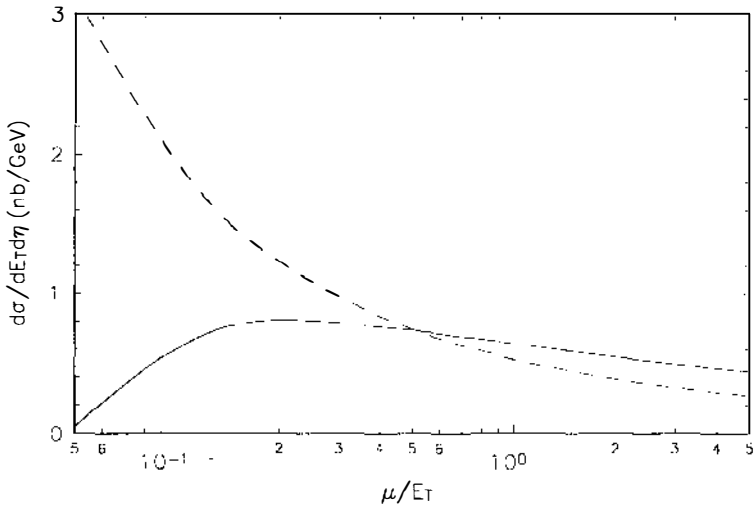

Figure 4 Sensitivity of a typical inclusive jet cross section ($\sqrt{s}$ = 1.8 TeV, E_T = 100 GeV, η = 0) to the renormalization scale for $O(\alpha_s^2)$ (dashed curve) and $O(\alpha_s^3)$ (solid curve) predictions. Note that near the hard scattering scale, E_t, the sensitivity is greatly reduced for the NLO calculation and the μ dependence goes from monotonic to forming a plateau near the hard scattering scale.

Several experimental jet algorithms have been employed. When cross sections are derived only at leading order and when uncertainties are large, these differences can be forgiven; even so, comparisons between experiments are rendered difficult. For example, UA1 (61) and CDF (63) employed cone algorithms, whereas UA2 initially used a nearest neighbor algorithm (62). A typical hadron collider algorithm is the "cone" algorithm, which has been suggested as a standard for $p\bar{p}$ experiments (64). It operates in a space defined by pseudorapidity and azimuth (η-ϕ) on particles, or partons or calorimeter towers, depending on the specific application. With these coordinates, one can define a jet to be the partons or particles found in cones or, more precisely, circles of radius $\Delta R \equiv \sqrt{\Delta\phi^2 + \Delta\eta^2}$. The transverse energy, E_t, is the sum of the transverse energies of particles, partons, or calorimeter towers inside a fixed radius. The direction of a jet in η and ϕ can be defined as the E_t weighted centroids:

$$E_t^{\text{jet}} = \sum_i E_t^i \qquad 3.$$

$$\phi_{\text{jet}} = \left(\sum_i E_{ti}\phi_i\right) \Big/ E_t^{\text{jet}} \quad 4.$$

$$\eta_{\text{jet}} = \left(\sum_i E_{ti}\eta_i\right) \Big/ E_t^{\text{jet}}. \quad 5.$$

The above description is not complete, however. It does not tell where to place the cones initially to form the above quantities, and it does not describe how to handle situations in which cones overlap ("merging"). In experiments employing calorimeters, the initial jet direction can be defined by towers with E_t above a given threshold (seed towers). An iterative approach can be adopted to find a stable center of the cluster by successively recomputing the cluster centroid until the list of towers or particles in the cone is stable (63). If two jets are more than one cone radius apart, but less than two radii (i.e. $R_0 < \Delta R_{1,2} < 2R_0$), should they be identified as one or two jets? The inherent difference between two partons in a calculation and calorimeter towers in an experiment can make it difficult to achieve a precise uniformity in the jet definition.

Both CDF (65) and the UA2 (51) experiments have measured jet cross sections using cone algorithms with $R = 0.7$ and 1.3 respectively, with reduced uncertainties. Although the UA2 results are not shown, there is good agreement with the $O(\alpha_s^3)$ predictions despite the fact that the calculations do not apply strictly for $R > \pi/3$ (59). The dominant experimental uncertainties are associated with the hadronic energy scale. The calorimeter response to jets, particularly the hadronic component, is difficult to calibrate in an absolute way. There are no test beams with monoenergetic sources of jets, so the calorimeter response must be derived from a convolution of the calorimeter response to hadrons of varying energy (including π^0's) with the jet fragmentation spectrum. Although the response can be checked with sources such as jets recoiling against direct photons, there is no unimpeachable source with which to calibrate. Typical energy scale uncertainties are now $\approx$4–15% in $\delta E/E$. A systematic shift in energy scale is equivalent to an uncertainty in the cross section. Since the cross section typically is a steeply falling function of E_t, following a power law spectrum of E_t^{-5}, the resulting uncertainty in jet cross section is 20–75%. Recent work by both the UA2 (51) and CDF (65) collaborations pressed the lower bounds of these uncertainties, thus improving the level of comparison to theory. The uncertainty can be expressed as an overall multiplicative factor that is independent of jet E_t (20% and 35% for CDF

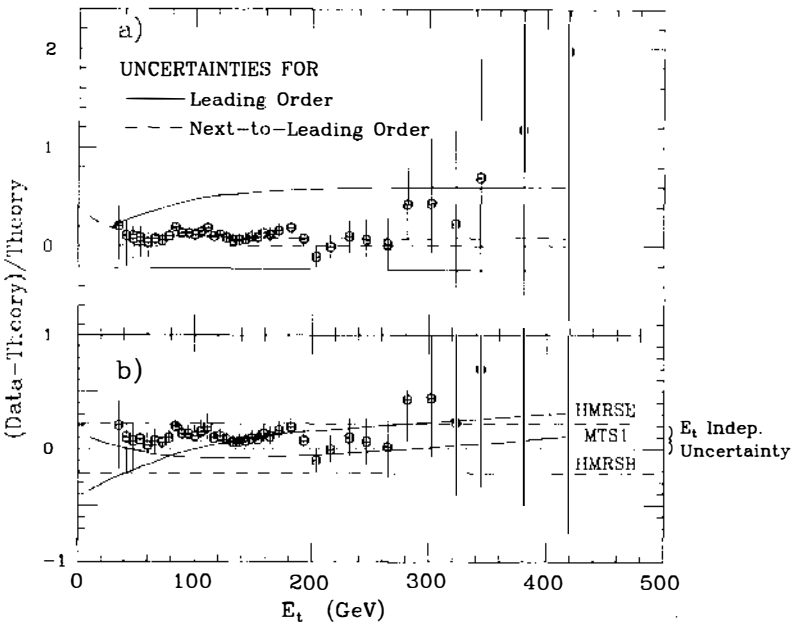

Figure 5 The inclusive jet E_t spectrum for CDF data using a cone size of 0.7, compared to theory as a ratio of (Data − Theory)/Theory. The upper plot (*a*) illustrates the theoretical uncertainty associated with variation of the renormalization scale μ ($E_t > \mu > E_t/4$) for both leading and next-to-leading order. The lower plot (*b*) illustrates the dependence on the choice of PDF. The $O(\alpha_s^3)$ prediction using the Harriman et al (31) set B PDF is used as a reference.

and UA2 respectively) and a smaller term that is E_t dependent and can be roughly 5% (65).

The agreement appears to be very good on a logarithmic scale. To illustrate significant features of the comparison, however, one can plot the cross section on a linear scale, as a ratio of (Data − Theory)/Theory as a function of jet E_t. Figure 5 shows such a comparison for CDF data (65). The QCD $O(\alpha_s^3)$ prediction for $\mu = E_t/2$ is defined to be the "Theory" or 0 on this plot for the purposes of normalization. The data have uncertainties factored into a combination of the E_t-dependent systematic and statistical uncertainties, which are displayed on the error bars, and an E_t-independent component, which is 20%. The top panel illustrates the improvement in the uncertainty associated with theory for a variation of $E_t/4 < \mu < E_t$. One can see that the uncertainties are substantially reduced at $O(\alpha_s^3)$. The bottom panel shows the effect of different PDFs on the predicted cross section (31, 33). As one can see there is some dependence on the shape of the derived cross

section on the choice of PDF; however, the overall agreement is quite good.

This does not exhaust comparisons at $O(\alpha_s^3)$. Figure 6 shows the variation of the cross section with cone size for E_t = 100 GeV jets from CDF compared with $O(\alpha_s^3)$ predictions (66–68). The data display the statistical errors only, but the ≈23% systematic uncertainties are largely independent of R. Since there are only two back-to-back partons in the leading order calculation, one can only predict such a variation beginning at next-to-leading order. An interesting feature of the calculation is the minimal sensitivity to μ for a cone size of R = 0.7, whereas the sensitivity is much greater both for $R < 0.5$ and $R > 0.9$. From this standpoint R = 0.7 represents an "optimal" cone size for comparison to $O(\alpha_s^3)$ predictions. The data appear to be in rough agreement with at least one of the QCD predictions ($\mu = E_t/4$), but on the whole, there seems to be a trend for the data to show a slightly steeper dependence on R than the theory predicts.

A quantity related to the variation of cross section with cone size is the jet profile. To measure this, one can pick a large radius (R = 1.0), and then examine the fraction of the jet E_t contained in a smaller subcone of radius r: $F(r,R,E_t)$. CDF measured this quantity using charged-particle tracking data because it is more fine-grained than calorimetric information. Figure 7 shows a plot of $F(r,R,E_t)$ from CDF data. Also shown are the predictions of $O(\alpha_s^3)$ QCD for different choices of renormalization scale (67). It is perhaps surprising that the data are so well described at the level of just one gluon bremsstrahlung when there are usually ten charged hadrons in a typical jet. Since $O(\alpha_s^3)$ is the

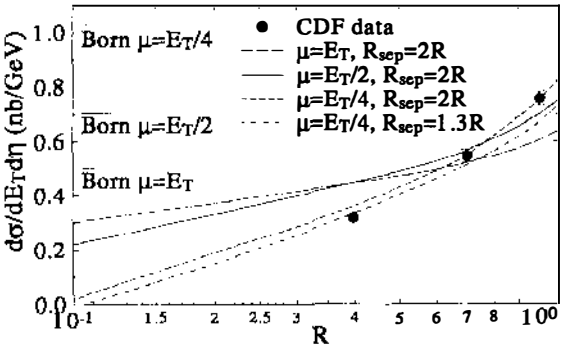

Figure 6 The variation of the jet cross section with clustering cone size R for jets of 100-GeV E_t. The standard $O(\alpha_s^3)$ calculation uses the merging parameter R_{sep} = 2.0, whereas a modified version employs R_{sep} = 1.3 (67).

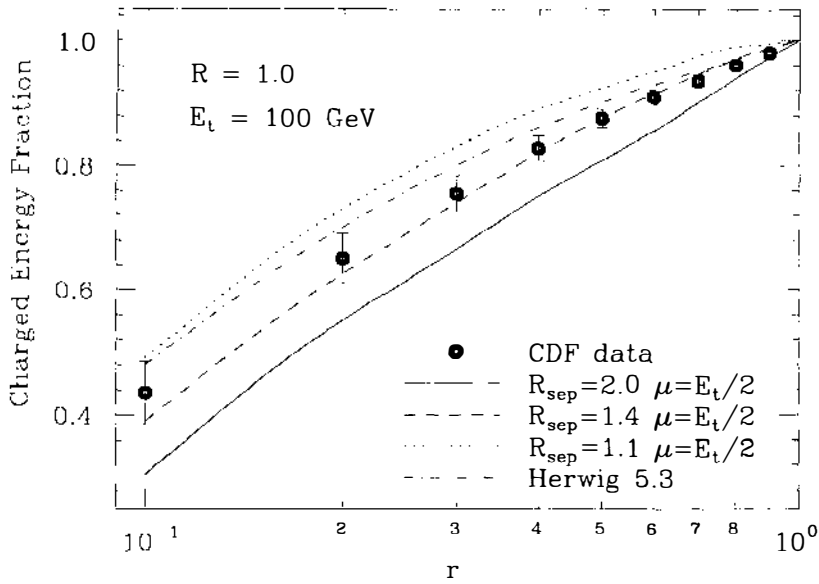

Figure 7 Fraction of energy contained in a subcone of radius r in jets found with a $R = 1$ cone. The data are from CDF charged tracking information, the QCD predictions are from Ellis et al (67) and from the HERWIG event generator (48).

lowest order at which one can speak of a jet profile, the sensitivity to renormalization scale is fairly large.

There is an apparent contradiction between the profile measurement and the variation of the cross section with cone size. One naively might expect that if there were good agreement between data and theory for one quantity, having chosen a renormalization scale, then there would be a good agreement for the other. This expectation is based on the assumption that the variation of cross section with cone size just depends on the energy flow within the cone. This assumption is not valid, however. In the inclusive measurement, jets are clustered independently for each chosen cone size, R, whereas for the jet profile, only a single cone of $R = 1.0$ is used. The main difference is the "merging" step. Ellis, Kunszt & Soper (67) examined the effect of merging in the $O(\alpha_s^3)$ predictions. As discussed above, there is an ill-defined region where two partons may be separated by a distance $R_0 < \Delta R < 2R_0$. In order to mimic the merging in the experimental algorithm, partons are merged into a single jet if they have a separation $\Delta R < R_{sep}$. The calculation implicitly had $R_{sep} \approx 2.0$. However, as seen in Figures 6 and 7 a value of $R_{sep} = 1.3$ and choice of $\mu = E_t/4$ fit both distributions

(67). Although consistent results are obtained, it is at the expense of adding a tunable parameter to the theory.

The ambiguities related to the prescription for the merging of jets are absent in the class of jet definitions generally used by the e^+e^- experiments. The prototype of these jet definitions is provided by the JADE algorithm, which builds clusters of charged particles according to an invariant mass cut (69). The invariant mass normalized by the center-of-mass energy, $y_{ij} = M_{ij}^2/E_{cm}^2$, is used to define jets as distinct objects. M_{ij} is the invariant mass of pairs of particles or of a particle and a cluster. At each step of an iterative procedure, the pair with the smallest y_{ij} is merged into a new cluster if $y_{ij} < y_{cut}$. If no pair is left passing the cut, all remaining clusters are called jets. The leading weakness of the JADE algorithm from the point of view of pp, $p\bar{p}$, and ep colliders is that all particles are associated to some jet, including those coming from the underlying event and those not belonging to the hard process.

Improved versions of the JADE algorithm have recently been proposed that reduce the sensitivity to the jet definition under hadronization corrections and make it possible to resume large classes of leading and subleading perturbative corrections in the theoretical calculations (70). These prescriptions can be extended to processes with hadronic initial states (71). In this formulation they provide an unambiguous prescription for the merging of jets and allow the universal factorization of initial-state collinear singularities, minimizing the contamination from the hadron remnants and the underlying event. The similarity with the e^+e^- jet definitions will make it possible to compare jet properties between e^+e^- and hadron colliders in a consistent and universal fashion. No complete phenomenological study of this new algorithm is available as yet, but we hope that progress will be made soon (S Ellis, Z Kunszt, and D Soper, personal communication) and that experimental measurements will follow as well.

3.2 x_t: *Jet Scaling with* s

If one plots the inclusive jet data in terms of two dimensionless variables, the "scaling" hypothesis predicts the scaled dimensionless cross section to be independent of $p\bar{p}$ center-of-mass energy, s. In reality, the evolution of PDFs and α_s with the hard scattering energy scale causes a violation of scaling for the inclusive jet cross section.

To test scaling, one typically plots E_t^4 times the invariant cross section ($E\,d^3\sigma/d^3p$) as function of $x_t \equiv 2E_t/\sqrt{s}$ to obtain two dimensionless quantities to express the jet cross section. If scaling were valid, cross sections measured in this way at any $\sqrt{s}$ would all fall on a single

universal curve. QCD, on the other hand, lifts the degeneracy. The predicted ratio of cross sections at two different center-of-mass energies as a function of x_t is relatively insensitive to choice of PDF, renormalization scale, or the order of the calculation, which makes it a relatively solid test of the theory. Independent measurements made at the Sp$\bar{p}$S, ISR, and Tevatron showed rough agreement with QCD scale breaking (51). The CDF collaboration recently compared jet cross sections at $\sqrt{s}$ = 546 and 1800 GeV as a test of x_t (72). When both cross sections are measured in one experiment, a large part of systematic uncertainties (e.g. hadronic energy scale) cancels when the ratio of the cross sections is taken, and thus the level of comparison is improved substantially.

Figure 8 shows the ratio of scaled cross sections as a function of x_t for CDF data taken at both center-of-mass energies. The error bars show statistical uncertainties, and the shaded area indicates an overall systematic uncertainty in the ratio. The data are clearly inconsistent with scaling (Ratio = 1). The data do not exhibit very good agreement with QCD either.

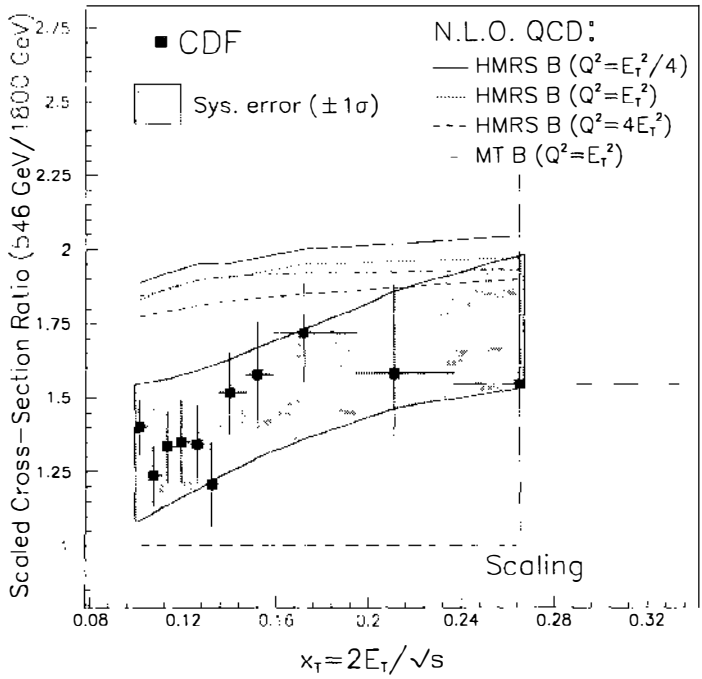

Figure 8 The ratio of dimensionless cross sections measured at $\sqrt{s}$ = 1.8 TeV and 0.546 TeV compared to QCD predictions at next-to-leading order.

The discrepancy with QCD is about two standard deviations in the systematic uncertainty, which is by no means sufficient to indict QCD, but it is curious. At the moment, there is no obvious explanation for such a discrepancy. PDFs in the relevant x range ($x > 0.1$) have been measured by a number of deep inelastic scattering experiments. Further running of the Tevatron collider at a lower center-of-mass energy could shed light on this.

3.3 *Two-Jet Distributions*

The $O(\alpha_s^3)$ predictions have been extended to measurements in which one defines a two-jet inclusive final state. Since soft radiation makes it impossible either to measure or to calculate states beyond leading order with two and only two jets, one can form quantities from the leading two jets and ignore other energy in the event. Ellis, Kunszt & Soper (60) recently extended the $O(\alpha_s^3)$ calculations to predict the two-jet-invariant mass and center-of-mass angular distributions. Such distributions are sensitive to the presence of deviations from QCD arising from quark compositeness, technicolor (73), and axigluons (74).

The CDF two-jet-invariant mass distribution M_{jj} is defined as:

$$M_{jj} = \sqrt{(E_1 + E_2)^2 - (\mathbf{p}_1 + \mathbf{p}_2)^2}, \qquad 6.$$

where E_i and $\mathbf{p}_i$ are the energies and momenta of jets $i = 1, 2$. Note that the effective masses of the jets enter into the determination of M_{jj}. The jet mass, an internal quantity, can be associated with gluon bremsstrahlung within the clustering cone. The CDF M_{jj} cross sections were determined for cone sizes of 0.7 and 1.0 (75). For the Harriman et al (31) and Morfin & Tung S1 (33) PDFs, the $O(\alpha_s^3)$ predictions improve significantly the comparison of data with theory. The agreement is very good for a clustering cone of 1.0. For a cone of 0.7 the rate is more sensitive to μ, and the shape to the choice of PDF. The agreement is fair for $\mu = M_{jj}/4 \cosh(0.7\,\eta^*)$, with $\eta^* = (\eta_1 - \eta_2)/2$.

The dijet angular distribution has likewise been calculated at $O(\alpha_s^3)$ (60). Since invariant mass and $\cos(\theta^*)$ are independent variables, the data can be placed in different bins of M_{jj}. Here θ^* is the center-of-mass polar scattering angle. Since the cross section is dominated by t-channel exchange, it rises very rapidly with increasing $\cos(\theta^*)$ and it is more convenient to plot the data as a function of the variable χ, defined as:

$$\chi \equiv \frac{1 + \cos\theta^*}{1 - \cos\theta^*}. \qquad 7.$$

If plotted versus χ, the Rutherford scattering pole is taken out. There is a rise in cross section for $\chi \approx 1$ (90°) associated with the contribution of s-channel scattering. Figure 9 shows the results of an analysis of $dN/d\chi$ by CDF using a cone size of 0.7 (76). The data are divided into three bins of M_{jj}. One can see that the data are well described by both $O(\alpha_s^2)$ and $O(\alpha_s^3)$ QCD predictions. The data are normalized separately for each bin of M_{jj}.

Quark compositeness would increase the number of events found near $\chi \approx 1$. Quark compositeness is typically parameterized in terms of a four-fermion interaction with a coupling inversely proportional to a characteristic energy scale (related to the "size" of the quark), Λ_c (65, 77). Such an interaction gives rise to an isotropic distribution in the center-of-mass system, and also contributes a rising cross section at large E_t or M_{jj}. In order to search for compositeness, one can take several bins of M_{jj} and examine the dijet angular distribution in each. Compositeness could be manifest as an increase in 90° scattering in the highest M_{jj} region, while the remaining data should be well described by QCD. The CDF data have allowed limits to be placed on $\Lambda_c > 1.4$ TeV using the inclusive jet data (65), and at $\Lambda_c > 1.0$ TeV using the angular distribution, as shown in Figure 10 (76).

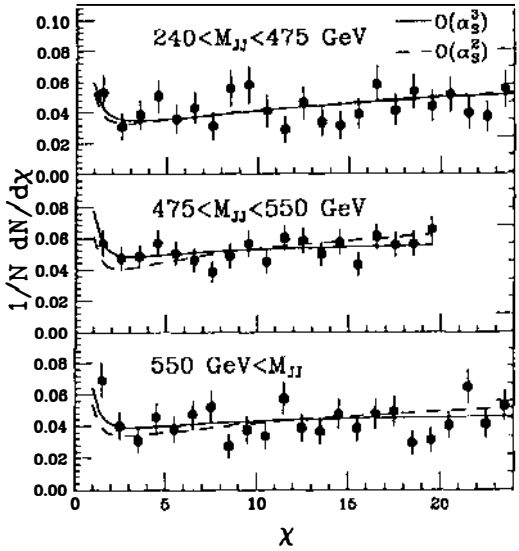

Figure 9 The dijet angular distribution, $dN/d\chi$ from CDF data (76) shown along with $O(\alpha_s^2)$ and $O(\alpha_s^3)$ predictions. The data are divided into three bins of dijet-invariant mass, M_{jj}.

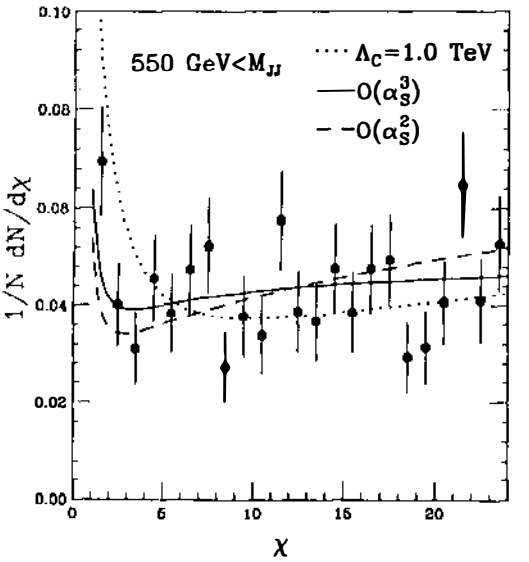

Figure 10 The dijet angular distribution from CDF data (76) for the highest values of M_{jj} compared with a model that includes both QCD and a parameterization for the effects of quark compositeness parametized by the scale Λ_c *(dashed line)*.

3.4 *Jet Fragmentation*

As discussed in Section 2, some aspects of jet fragmentation reveal the underlying QCD mechanisms, particularly when one assumes that the behavior of hadrons in jets mimics features of the partonic emission. On this basis, one expects, for example, that gluon jets will have softer fragmentation than quark jets and that average multiplicities will increase with energy.

Studies of jet fragmentation in hadronic collisions have been performed in the past by UA1 and UA2, providing the first indications that jets in $\bar{p}p$ reactions have higher multiplicities than in e^+e^- annihilation (78).

The most notable quantity to study is the jet fragmentation function, which describes the probability of finding a hadron carrying a given fraction of the jet's momentum. This is typically described in terms of the component of hadronic momentum parallel to the jet axis: $p\|$. The charged-particle fragmentation function, $F(z)$, is defined as ($z \equiv p\|/p_{\text{jet}}$):

$$F(z) = \frac{1}{N_{\text{jet}}} \frac{dN_{\text{ch}}}{dz}. \qquad 8.$$

The evolution of $F(z)$ as a function of the hardness of the primary collision is a good test of QCD, and, in principle, can be used to extract α_s. The same mechanism for the evolution of parton densities, namely soft and collinear parton emission, is responsible for the logarithmic evolution of $F(z)$. Figure 11 shows the evolution of different bins of $F(z)$ as a function of dijet-invariant mass (M_{jj}) from CDF data (79). The data agree well with a logarithmic evolution with M_{jj} and show a distinct similarity to e^+e^- data from TASSO (80), which are plotted in Figure 11 as a function of s. M_{jj} appears to be a sensible variable to express this evolution insofar as it is a measure of the hardness of the scattering, particularly in the central pseudorapidity region.

Notice however that the e^+e^- and $\bar{p}p$ curves do not match: the e^+e^- curve corresponding to the lowest z bin extrapolates below the equivalent CDF curve. This behavior is consistent with the notion that jets in hadronic collisions are produced mostly by gluons, while in e^+e^- they come from the evolution of quarks. We should, however, point out that jets are defined according to different algorithms in e^+e^- and hadronic collisions (Section 3.1), and unless a common definition is provided it is not possible to draw quantitative conclusions from these comparisons. Nevertheless it is encouraging that, as shown by Abe et

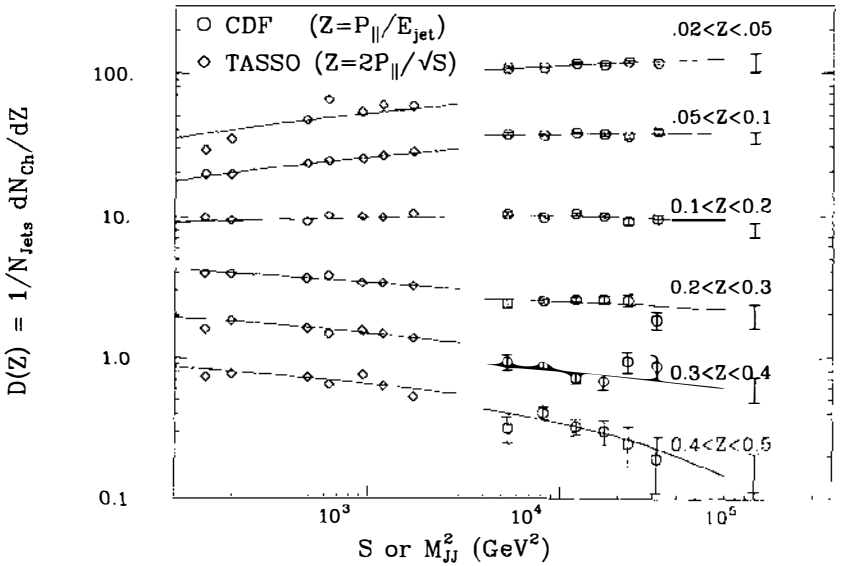

Figure 11 The evolution of the jet fragmentation function, $F(z)$. Data are from CDF (79) and TASSO (80). This is shown along with fits of the form $A \ln M_{jj} + B$ (79).

al (79), calculations based on the HERWIG Monte Carlo are in agreement with the measured inclusive fragmentation function.

3.5 *Multijet Final States*

In all of the above, one has considered final states in which two jets predominate. Predictions for multijet final states are obtained either from QCD shower Monte Carlo programs or from fixed-order perturbation theory. For the latter, one can obtain finite cross sections by limiting the minimum E_t and opening angle of partons in order to avoid soft and collinear singularities. For selected states in which the partons are stiff and widely separated, one expects tree-level predictions to be reasonably faithful. There is no NLO calculation available for $N_{jet} > 2$; therefore, since one does not have the $\log(\mu)$ cancellation that appears at NLO, there is a substantial sensitivity in the predicted cross sections to a variation of the renormalization scale. This is because the cross section is of order $\alpha_s(\mu)^N$, where N is the number of final-state partons. Any uncertainty in the scale will hence be multiplied by a large factor in deriving cross sections.

The tree-level matrix elements commonly in use are based on calculations by several groups[2] and have been included in the numerical programs currently used by the experiments (82, 83). Because of the complexity of the results, techniques have been developed to provide reliable approximations of these matrix elements (84–88). Testing of these approximations against current data is very important because rates for multijet production at the future colliders will be extremely large and fast, but reliable numerical simulations will be required to evaluate them.

To start with, the topologies of multijet final states appear to be well predicted by the tree-level calculations. Several examples can be seen in both CDF and UA2 data. CDF examined the topology of three-jet events with high statistics and in regions of uniform acceptance. They found a very good agreement with tree-level predictions (63). In particular, there is a distinct difference expected between three-jet topologies for events initiated by gluon-gluon and gluon-quark collisions versus those from quark-antiquark collisions. The data appear to be in good agreement with the expectation that most of the three-jet final states come

Both UA2 and CDF explored in some detail the structure of four-jet final states (89, 90). These studies are motivated partly by a search for double-parton processes in which two uncorrelated $2 \rightarrow 2$ scatters

[2] For a review of these techniques and for a complete set of references, see (13).

occur, producing four jets in the final state. Figure 12 shows the angular separation of all pairings of jets from four-jet events in CDF data (90) and compares them with the results of predictions based on the exact tree-level matrix elements (82), which reproduce the data very well. In contrast to QCD production, where the four jets have no intrinsic correlation, the double-parton events are expected to have jet pairs that approximately balance in transverse momentum. One expects that the cross section for double-parton events would scale like the square of the dijet ($2 \rightarrow 2$) cross section, normalized by a factor that is comparable to the inelastic cross section (81):

$$\alpha_{DP} = \frac{\sigma_{dijet} \times \sigma_{dijet}}{2\sigma_{eff}}, \qquad 9.$$

where σ_{eff} is expected to be roughly 10 mb (90). The factor of two in the denominator is included to account for the Poisson-like character of a double-parton interaction (92). The Axial Field Spectrometer (AFS) collaboration reported a significant double-parton cross section, with $\sigma_{eff} = 5$ mb (91), whereas the UA2 collaboration did not find any evidence for the process and set a limit of $\sigma_{eff} > 8.3$ mb (95% CL)

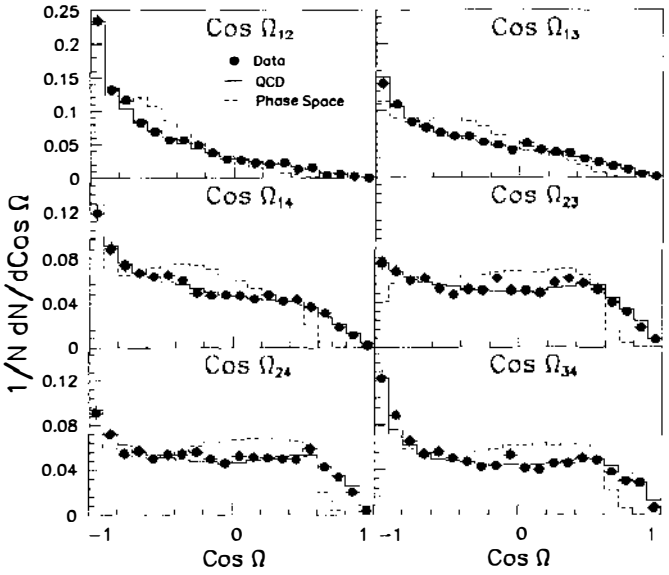

Figure 12 Angular separation for pairs of jets in four-jet events. The solid line shows the predictions from exact leading order QCD matrix elements (82), and the dashed line represents the expectations of phase space. The tree-level predictions clearly describe the data much better than does phase space. Jets are ordered by p_t (90).

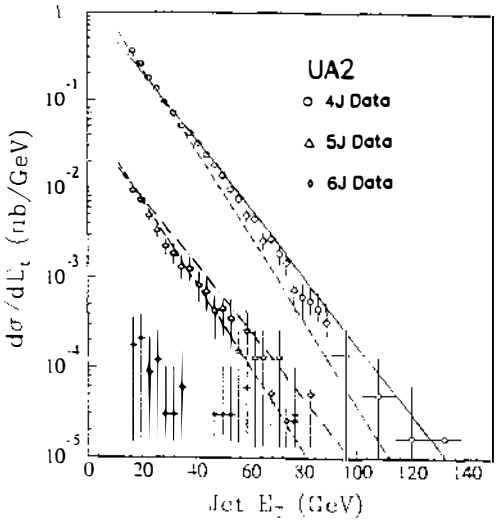

Figure 13 The distribution of jet p_t for 4-, 5-, and 6-jet events from the UA2 collaboration (89). The solid curve represents the exact leading order QCD calculation for four jets (82, 83). The dashed-dotted line is the result of the Maxwell approximation for five jets (87), and the dashed lines are the predictions using the Kunszt-Stirling approximation (86).

(89).[3] Note that since σ_{eff} appears in the denominator of Equation 9, a larger number implies a smaller σ_{DP}. Finally, CDF reported an effect at a level of roughly 2.5 standard deviations, with $\sigma_{\text{eff}} = 12.1^{+10.7}_{-5.4}$ mb. For four-jet final states at the SSC, double-parton scattering is expected to dominate for jet p_t's less than 40 GeV (90). If in the future a sizable effect is observed, it is possible one may obtain unique information on correlations between partons in the proton from double-parton scattering.

The UA2 collaboration studied the cross section of events with up to six jets. Figure 13 shows the jet p_t distributions for 4-, 5-, and 6-jet final states, compared with various tree-level predictions. Notice that the normalization of the theory curves is absolute. Considering the complexity involved in these calculations, the agreement with data is remarkable and extremely encouraging in view of the potential applications of these calculations to the study of multijet phenomena at the future hadronic colliders LHC and SSC.

[3] The findings by UA2 and AFS are not necessarily inconsistent: on one side, the x range probed by the multijet configurations at the two energies of 63 and 630 GeV is very different. On the other, at the time of the AFS analysis the exact predictions for the QCD four-jet production were not available.

As an alternative to exact tree-level calculations, and to get a more exclusive description of the events, one may employ shower Monte Carlos. In this approach multiple jets can appear when branchings with large transverse momentum relative to the leading partons take place. Given the approximations involved in evaluating these large p_t branchings inside the Monte Carlo, the reliability of this approach should be assessed.

CDF recently performed a detailed comparison of the characteristics of events with high total transverse energy with the HERWIG event generator combined with a realistic detector simulation (93). The events were selected by requiring that the total transverse energy be in excess of 400 GeV. Events with up to six jets were observed, and the HERWIG generator does an impressive job in reproducing a very large number of distributions, such as the jet multiplicity as a function of different jet-p_t thresholds (Figure 14), the jet profiles, and invariant masses of various combinations of jets. Such studies illustrate the power and accuracy of event generators in reproducing event characteristics.

Although they agree in rough detail, there are some significant differences among some of the Monte Carlo event generators. One of the

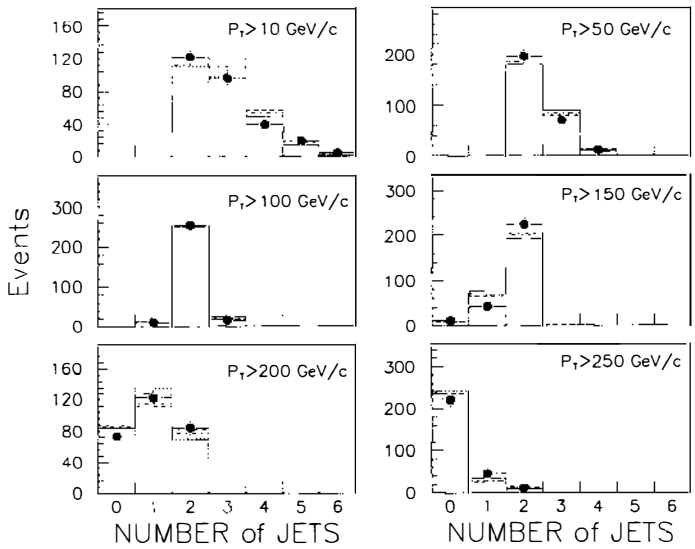

Figure 14 The jet multiplicity plotted for different minimum jet p_t cuts for events with greater than 400 GeV total transverse energy from CDF data (93). The histograms are from the HERWIG event generator combined with a detector simulation. Each histogram represents a different choice of PDF; employed were DO1 *(solid)*, DO2 *(short-dashed)* (94), EHLQ1 *(long-dashed)* and EHLQ2 *(dot-dashed)* (15).

most relevant differences is how color flow is handled. In particular, the dynamics of color flow necessitate angular ordering of QCD radiation in shower Monte Carlos (10). The emission of radiation is related to the color structure of the hard scattering process. Some event generators, such as ISAJET, ignore the connection between radiation and the hard scattering, whereas other generators, such as HERWIG, have explicitly incorporated the color flow to reproduce better event properties. The differences between coherent and incoherent emission have been studied extensively in e^+e^- (14), but not as much in $p\bar{p}$ collisions, largely because of the inherent problems in distinguishing the soft particle flow associated with the hard scattering from that associated with the underlying event. For sufficiently large momentum transfers, however, one expects the radiation effects to become visible as jets, which are more readily associated with the hard scattering process. CDF studied the angular distribution of the third highest E_t jets in events with two high E_t leading jets (95). These studies show significant differences between the predictions for ISAJET and HERWIG; the data are in much better agreement with HERWIG, which indicates that, for some measurements, color coherence effects cannot be neglected.

4. HEAVY FLAVOR PRODUCTION

Heavy quark production in high energy hadronic collisions constitutes a fundamental arena for the study of perturbative QCD. Of particular importance is the role played by m_Q. Only in b quark production does one find today the unique situation in which $m_Q \gg \Lambda_{QCD}$. The prediction of heavy quark production cross sections in hadronic collisions has far-reaching implications. Discovery reaches and limits for the "top" quark depend on reliable estimates from perturbation theory. The observability of *CP* violation in B mesons at hadron colliders depends, to a large extent, on the production cross section and correlations between the B and $\bar{B}$ (96). Recent years have witnessed remarkable progress both in the theoretical understanding of the production mechanisms (97) and in the experimental capability to probe them via independent and complementary observations (98).

The mass of the heavy quark Q provides a natural infrared cutoff in the evaluation of the production rates and multiplicities. Complete next-to-leading order calculations are available today for the total (99), one-particle-inclusive (100), and two-particle-inclusive (101) cross sections. Production of heavy quarks in the perturbative evolution of high

energy jets has also been studied, and leading order expressions for the heavy quark multiplicities are known (102).

The nonperturbative corrections required to derive the production properties of observable heavy flavored hadrons h_Q are suppressed by powers of Λ_{QCD}/m_Q. For production at large p_t, the factorization theorem guarantees the existence of a fragmentation function $D^Q_{h_Q}(z,\mu)$, which models the fraction of momentum of the heavy quark retained by the heavy hadron:

$$\frac{E\, d^3\sigma_{h_Q}}{d^3p} = \int \frac{E'}{d^3p'}\frac{d^3\hat{\sigma}_Q}{} D^Q_{h_Q}(z,\mu)\,\frac{dz}{z^2}, \qquad 10.$$

where $p = zp'$ and $\hat{\sigma}_Q$ is the elementary cross section for the production of the heavy quark Q, calculable as a perturbative expansion in α_s. The evolution of the fragmentation function with the factorization scale μ obeys the Altarelli-Parisi equation (23) with a boundary condition given by $D^Q_{h_Q}(z,m_Q) = \delta(1-z)$, up to nonperturbative effects (103). These nonperturbative effects obey a scaling law in m_Q and can therefore be parametrized in a phenomenological way by fitting, for example, e^+e^- data (104, 105). With this additional input, nonperturbative corrections to Equation 10 are suppressed by powers of p_t. The evolution of $D^Q_{h_Q}(z,\mu)$ with μ is known today up to next-to-leading order in perturbation theory (106).

When applied to the energy of the current hadron colliders, these results are believed to provide a reliable description of the production properties of very massive quarks, for example the yet undetected top quark. In the case of charm and bottom quarks, the situation is more delicate. In fact, production of c and b quarks is dominated by gluon fusion processes ($gg \rightarrow Q\overline{Q}$), and the distribution of gluons inside the proton is probed at values of x close to the boundary of current DIS measurements. Furthermore the next-to-leading order contribution is larger than the leading order result, and very sensitive to the input scale μ. Significant corrections are thus expected from yet higher order terms. These corrections arise from a class of diagrams with t-channel gluon exchange first appearing at next-to-leading order (107) (Figure 15). They lead to terms proportional to powers of $\alpha_s \log(s/m_Q^2)$, which might dominate at higher energies, as well as becoming nonnegligible in top production at supercollider energies (99). Techniques exist to resum these large logarithms (108) and have been extended for application to this specific problem (109–111). Comparing the results of the next-to-leading order predictions with the available data and verifying whether the resummed calculations can explain possible differences

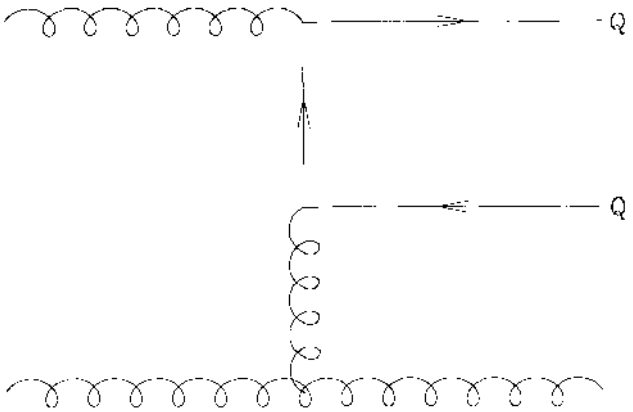

Figure 15 A representative diagram for the *t*-channel gluon exchange contribution to heavy quark production.

are therefore of utmost importance as a test of QCD per se and as a milestone before extrapolation to higher energies.

4.1 *Bottom Production*

Bottom quarks can be detected in several different channels. Fully reconstructed exclusive decays of b hadrons allow the unambiguous tagging of a b quark, together with a precise measurement of the hadron momentum. Viable examples are provided by $B^{\pm} \rightarrow J/\psi K^{\pm}$ (113, 114), $B^0 \rightarrow J/\psi K^*$ (115), and $\Lambda_b \rightarrow J/\psi \Lambda$ (113). Because of the small branching ratios (BR) and detection efficiencies, these channels are only accessible near threshold [$p_t = O(m_b)$], where the production rate of b quarks is more abundant. The region of small p_t is expected to be more sensitive to the uncertainties in the calculations mentioned previously and is therefore potentially more interesting for critical tests of QCD.

At larger values of p_t (typically above 10–15 GeV), semileptonic decays become the leading tool to study b production. Neglecting detector backgrounds and neglecting W, Z, and c decays, one finds b quarks to be the most abundant source of high p_t leptons. Several techniques can be employed to subtract the above backgrounds (98). Backgrounds from Z's, W's, and continuum Drell-Yan events can be identified because single leptons from these processes are more isolated than leptons from heavy quark decays, which are surrounded by the fragments of a jet. In addition, lepton pairs from Z's can be eliminated with a cut on the invariant mass of the lepton pair, and W's can be identified by the large transverse mass of the $\ell\nu$ pair.

For p_t values larger than 10–15 GeV, the c and b cross sections are

comparable. Since b quarks undergo a harder fragmentation into hadrons than do c quarks, and since b hadrons have a larger phase space available for the decay, we expect the c contamination to contribute only a small fraction of the total lepton yield. This fraction can be precisely estimated by studying the transverse momentum of the lepton relative to the direction of the jet in which it is imbedded (112).

Furthermore, the b component can be determined by tagging charmed hadrons (say D's) inside the jet and with the correct charge correlation with the lepton itself, e.g. $e^- D^0$ as opposed to $e^- \overline{D}^0$. UA1 has pioneered a technique based on the detection of a second lepton in the event (112). This second lepton comes either from the charm quark emitted during the decay of the b into the leading lepton, or from the decay of the second b in the event. In the first case, we have a low mass dilepton pair, and the measured rate can be directly related to the b cross section. In the second case, we have a high mass dilepton pair, and the extraction of the inclusive b cross section requires an understanding of the correlations between the two heavy quarks in the event (120).

New technologies, such as secondary vertex detectors capable of isolating the charged particles coming from the displaced vertex of a B decay, will provide more tools to strengthen the capability of hadron collider experiments to tag b hadrons and study their properties.

Unlike other inclusive measurements (e.g. direct photon, jet production), inclusive b cross sections are reported as the integrated cross sections for all events with p_t' greater than p_t. This is done to minimize systematics associated with the b fragmentation and decay. The effects of these two processes must be unfolded in order to obtain a b cross section from the observed lepton spectrum. The results of the measurements by UA1 (112) and CDF (114–116) are collected in Figure 16. The two solid lines represent the NLO QCD prediction (100), obtained using PDFs from the most recent fit from Martin et al (34) (set D0) and two different values for μ and $\Lambda_{\overline{\rm MS}}$.[4] This band is supposed to represent an acceptable range of variation for the input parameters of the NLO calculation. The value of m_b was fixed at 4.75 GeV. A variation of the mass in the range $4.5 < m_b < 5$ GeV affects the result by no more than 20% in the region $p_t < 10$ GeV, and by only of the

[4] It is worth pointing out that the values of $\Lambda_{\overline{\rm MS}}$ extracted from fits to DIS data are systematically lower than those obtained from precision measurements of jets performed at LEP (117). The differences are of the order of two standard deviations. Use of the α_s extracted from LEP experiments would increase the predicted b cross sections by an additional 20%.

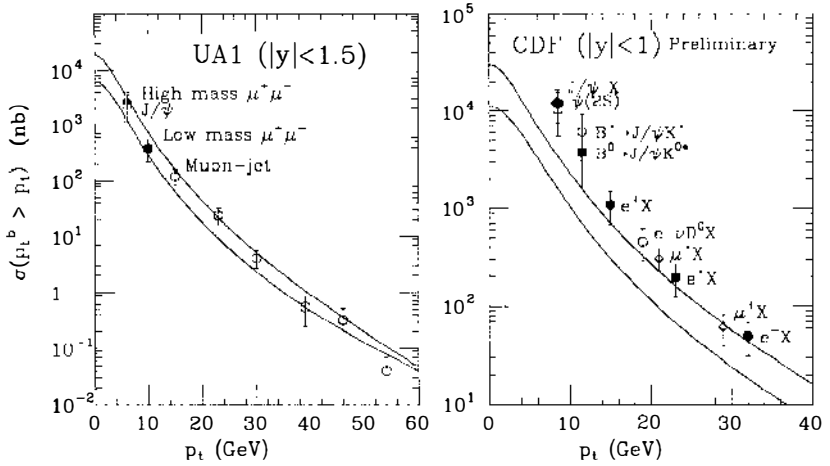

Figure 16 Integrated b p_t distribution at UA1 *(left)* and CDF *(right)*: data versus NLO QCD. The lower curves correspond to $(\mu, \Lambda_{QCD}) = (m_T, 215\ \text{MeV})$, the upper ones to $(\mu, \Lambda_{QCD}) = (m_T/4, 275\ \text{MeV})$, with $m_T^2 = p_t^2 + m_Q^2$. 275 MeV corresponds to one standard deviation from the central value of the MRSD0 fit for $\Lambda_4^{(2)}$.

order of few percent above 20 GeV. Two features are to be noticed. First of all, the theoretical uncertainty is rather large, significantly larger than the uncertainties encountered in the case of the NLO inclusive jet cross section. Secondly, while the UA1 data fall well inside the theoretical band, the CDF points are systematically higher, with deviations of up to a factor of three for the low p_t points.

No satisfactory explanation for this discrepancy is yet available, though at least two suggestions have been put forward. First, the gluon momentum fractions x probed by the CDF measurements are significantly smaller than those probed by UA1. Attempts have been made explicitly to include the CDF b data in global fits of the gluon density (118). These attempts have not led to a complete solution of the problem. An explanation of this shortcoming can be found in the following observation (119): the region in x that is unexplored even by the most up-to-date DIS data is $x < 0.01$; using the available extrapolations of the gluon densities below this value, one finds the contribution to the cross section for b's with $p_t > 10$ GeV coming from the region $x < 0.01$ is only of the order of 20% (Figure 17). Therefore only large differences in the extrapolation could explain the observed discrepancy, and such differences are difficult to achieve because of the global constraints posed by the measurements of gluon distributions at larger values of x, such as momentum sum rules.

An alternative explanation could be provided by the presence of the

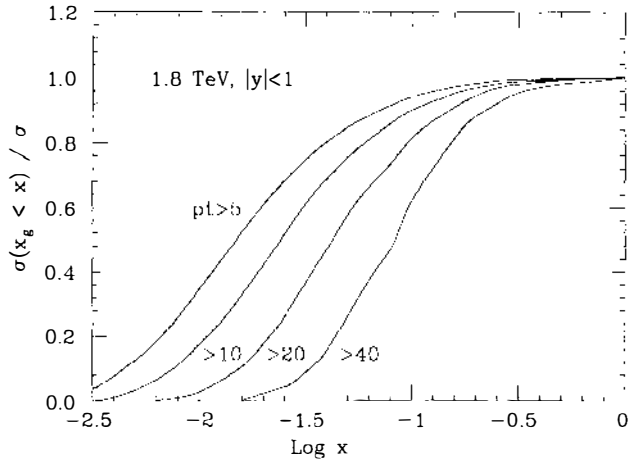

Figure 17 Fraction of the NLO QCD b cross section at 1.8 TeV coming from gluons with $x_g < x$, for different p_t thresholds.

large $\log(s/m^2)$ corrections mentioned previously. Several studies have led to a general reformulation of the factorization theorem for application to processes involving initial-state gluons with small momentum fraction x (109–111). The result can be expressed in terms of gluon distributions depending not just on x and μ, but on the transverse momentum $\mathbf{k}$ as well (109):

$$\sigma(s) = \int_0^1 dx_1 \int_0^1 dx_2 \int_0^\infty d\mathbf{k}_1^2 \int_0^\infty d\mathbf{k}_2^2 \, \mathcal{F}(x_1,\mathbf{k}_1,\mu)\mathcal{F}(x_2,\mathbf{k}_2,\mu) I(\hat{s},\mathbf{k}_1,\mathbf{k}_2), \quad 11.$$

where the functions $\mathcal{F}$ describe the transverse momentum distribution of gluons with longitudinal momentum fraction x. I, referred to in the literature as the impact factor, represents the gauge-invariant elementary cross section for the process $gg \rightarrow Q\overline{Q}$ with initial off-shell gluons of virtuality $-\mathbf{k}^2$. An intuitive physical interpretation of this result is the following: at small x and for $\mu \gg \Lambda_{QCD}$, gluons are more likely found in a peripheral branch of the initial-state evolution tree. In other words, the multiplicity is dominated by processes in which the degradation of the gluon momentum down to a fraction x took place via a large number of successive splittings (see Figure 18). Since at each splitting the gluon acquires some transverse momentum $\mathbf{k}$, $\mathbf{k}$ will build up during the evolution to small x; for x small enough, the transverse momentum will not be negligible with respect to the scale of the hard

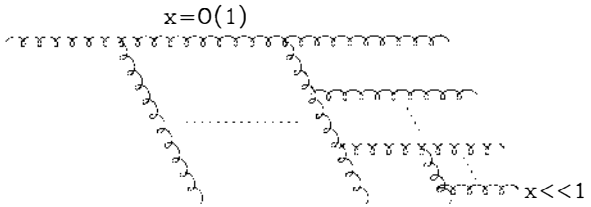

Figure 18 A picture of the evolution of a gluon toward the small-x region.

process, μ. Therefore the description of the gluon density at small x should depend on $\mathbf{k}$ as well as on x and μ, and its evolution equation cannot neglect the transverse degree of freedom. An evolution equation for the density $\mathcal{F}(x, \mathbf{k}, \mu)$ extending the standard Altarelli-Parisi equation can be formulated (108). This evolution equation resums the leading $[\alpha_s \log(s/m^2)]^n$ terms that appear in the perturbative expansion for the hard scattering cross section and allows them to be absorbed into $\mathcal{F}(x, \mathbf{k}, \mu)$, provided one uses the impact factor I rather than the standard on-shell matrix element in the expression for the cross sections, Equation 11. The result of this approach cannot be simply estimated by varying the renormalization scale μ within some range, because the impact factor and the $\mathbf{k}$-dependent density contain information beyond what available in the standard NLO calculation; this could explain why even the change of μ in the rather extreme range of $m_T/4 < \mu < m_T$ cannot reconcile the NLO prediction with the data.

The main physical consequence of this picture is that small-x gluons involved in a hard scattering at a scale μ will have an intrinsic transverse momentum of the order of μ itself. This additional transverse momentum will smear the p_t distributions obtained from a pure NLO calculation, but complete calculations of this effect are not yet available. Explicit estimates exist of the corrections to the total cross section resulting from Equation 11 (109). At Tevatron energies, these corrections amount to approximately 50% of the NLO total cross section. While this effect seems insufficient to explain the observed discrepancy, one should keep in mind that the smearing induced by the effective intrinsic p_t introduced by Equation 11 could very well push most of this contribution to values of $p_t > m_b$, where the NLO cross section is only a fraction of the total.

While we await more calculations, it is worth exploring additional consequences of this scenario. In addition to pushing the measurement of b quarks to smaller values of p_t, it is useful to study correlations between the b pair. NLO calculations exist for these correlations (101). If the small-x effects behave as indicated, we would expect to observe

a flattening of the $\Delta\phi$ and $p_t^{b\bar{b}}$ distributions relative to the NLO prediction. Here $\Delta\phi$ represents the difference in azimuth between the b and the $\bar{b}$, and $p_t^{b\bar{b}}$ represents the transverse momentum of the pair. The flattening would be caused by the additional intrinsic p_t from the gluon transverse momentum **k**.

The $\Delta\phi$ correlations have been studied by UA1 and show good agreement with the NLO calculation (120). This result does not resolve the issue; the agreement of the NLO b cross section with the data may be because the energy at UA1 is below the threshold for the possible onset of these new small-x phenomena.

4.2 *Charmonium Production*

In this section we review the status of the measurements of production cross sections for charmonium resonances such as the J/ψ. The theory of quarkonium production (121) is on a less solid ground than the theory of open heavy quark production. Production cross sections are evaluated by convoluting the $c\bar{c}$ matrix elements with the nonrelativistic charmonium wave function, parametrized in terms of the decay widths of the relevant (J, L) state. The QCD radiative corrections to the leading order processes have not yet been evaluated.

The observation of J/ψ's is, however, an important ingredient in the study of b production. On the one hand, a significant fraction of the detected J/ψ's comes directly from b-hadron decays rather than from prompt charmonium formation (122, 123). In fact, the J/ψ form factor inhibits production with $p_t \gg m_c$. On the other hand, b-decay final states involving a J/ψ provide unique tags in the search for yet unobserved or rare b hadrons (such as B_s, B_c, Λ_b) as well as in the detection of CP asymmetries, e.g. from $B_d \rightarrow J/\psi K_S^0$ decays (96). A coherent picture of the production of both b and J/ψ in hadronic collisions will therefore provide not only a significant test of QCD, but also the starting point for important studies of the Standard Model.

Figure 19 shows the inclusive p_t differential distribution for J/ψ's measured by UA1 (123) and CDF (124). We superimpose the result of a QCD calculation (119) based on leading order matrix elements (121) for the direct charmonium production, plus the contribution from B decays evaluated using NLO matrix elements (100), convoluted with a Peterson fragmentation function and the experimentally observed $B \rightarrow J/\psi$ decay spectrum. The theoretical error band is evaluated using the same range of parameters Λ_{QCD} and μ employed before in the study of the b cross sections. Notice that changing μ for the direct charmonium contribution creates a variation ranging from a factor of 7 to 10, depending on p_t. This indicates that the leading order prediction

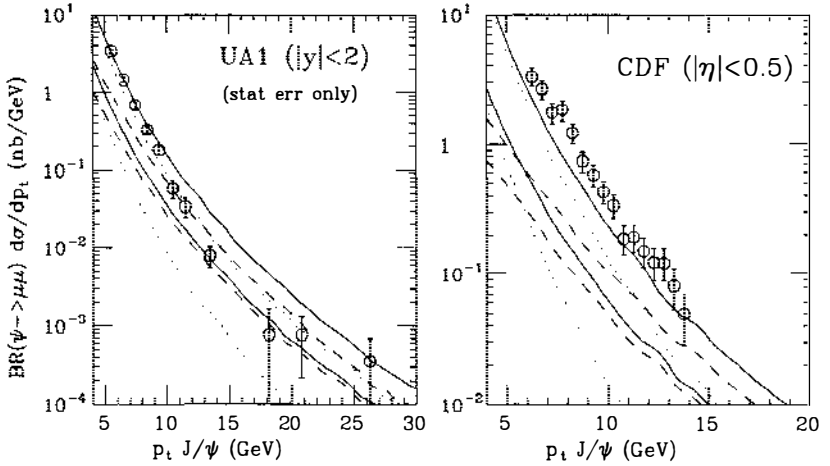

Figure 19 J/ψ p_t distribution at UA1 *(left)* and CDF *(right)*: data versus QCD. *Dotted line:* direct quarkonium. *Dashed line:* b decays. *Solid line:* total. The lower set of curves corresponds to (μ, Λ_{QCD}) = (m_T, 215 MeV), the upper set to (μ, Λ_{QCD}) = (m_T/4,275 MeV). Parton distribution set MRSD0 (34).

for direct charmonium is very poor, and very large next-to-leading order corrections should be expected.

In the case of UA1, all the data fall inside the theoretical band, while again CDF shows a production rate larger than expected. A similar feature is observed in the CDF measurement of the ψ(2S) p_t distribution (124).

An important parameter is the fraction of J/ψ's coming from b decays, f_B. This number allows us to extract a b cross section from the observed J/ψ production rate. Notice from the theoretical curves in Figure 19 that f_B is very sensitive to the parameters used for the evaluation of the two contributions.

The fraction f_B can be extracted experimentally: for example, one can separate the J/ψ's produced directly from those due to B decays by observing the displaced vertex from which the J/ψ originates, the displacement resulting from the long B lifetime. UA1 measured f_B by assuming that direct J/ψ's are isolated while J/ψ's from B decays are not. They obtained 32% for $p_t(\psi) > 5$ GeV (123). This number is consistent with the estimates provided by Mangano (119).

The assumption used by UA1 to extract f_B might not be correct if other production mechanisms were responsible for direct quarkonium production, such as gluon → J/ψ fragmentation (127). It is reasonable to expect that at some value of p_t the dominant production mechanism for charmonium states will indeed be gluon fragmentation. The main

rationale is that direct production as described by the leading order mechanisms inhibits production at large p_t via a form factor suppression (the probability that a charmonium bound state will hold together when produced directly in an interaction with a large virtuality scale is highly suppressed). The fragmentation functions for the creation of S-wave charmonium (η_c and J/ψ) in a gluon shower have recently been calculated (127), and those for the creation of P-wave states (χ) will soon be available (E Braaten and TC Yuan, personal communication).

These calculations can be used to extract the fragmentation contribution to charmonium production in the regions of p_t explored experimentally, and to verify whether this process can account for the large observed rates. The experimental detection of nonisolated J/ψ's from a primary vertex, and therefore not coming from B decays, would indicate that these processes are indeed present.

Measurements of the decay vertex position of the ψ(2S) would provide evidence for or against the current belief that most of them come from B decays. If the gluon fragmentation mechanism were important, it would appear with a signal of nonisolated prompt ψ(2S).

Similarly interesting would be a measurement of the χ_c p_t spectrum, which is expected to be dominated by direct production rather than B decays. A preliminary measurement of CDF reports $BR(\psi \rightarrow \mu^+\mu^-) \times \sigma(\chi_c \rightarrow \psi\gamma; (p_t)_\chi > 7\ \text{GeV}; |\eta| < 0.5) = 3.2 \pm 0.3 \pm 1.2$ nb (125). Both χ_1 and χ_2 are here included. This value can be compared with the range of $0.64 < \sigma < 5.1$ nb obtained using the leading order QCD calculation described above (119). Using the above cross section and the inclusive $B \rightarrow \chi_{c1}$ branching ratio of $0.54 \pm 0.21\%$ (128), we estimate that fewer than 10% of the χ's come from B decays.

A measurement of the production cross section and p_t spectrum for Υ states would also be very useful in understanding the quarkonium production mechanisms. In this case, one has at least three advantages: (*a*) the masses involved are larger and presumably both the nonrelativistic approximation involved in the determination of the quarkonium wave function and the QCD perturbation theory would work much more reliably than for charmonium; (*b*) the signal is not contaminated as is the one from B decays; and (*c*) the p_t spectrum could be extended to very small values of p_t, thanks to the large mass of the Υ and the large momentum of the decay muons.

5. W AND Z PRODUCTION

5.1 *Inclusive Measurements*

Inclusive production of W and Z bosons is the most accurately known process in hadronic collisions. The absence of final-state strong inter-

actions affecting the observed state, one or two large-p_t charged leptons, allows for high precision measurements and calculations. Uncertainties in the measurement of the total cross sections (129, 130) are less than 10% and are dominated by the uncertainty on the absolute luminosity (see Table 1). The full next-to-next-to-leading order $O(\sigma_s^2)$ corrections to the cross section are known (131), and techniques for the resummation of classes of leading and subleading logarithmic corrections to all orders of perturbation theory are available (132). The current theoretical systematic error is below 5%, estimated by varying factorization and renormalization scales within the range $10 < \mu < 1000$ GeV. Slightly larger uncertainties arise from the use of different PDFs. The agreement between theory and experiment, at both Sp$\bar{p}$S and Tevatron energies, is within one standard deviation and does not favor any particular set of PDFs provided one uses recent NLO fits. Even though the $O(\alpha_s^2)$ corrections add only a very small numerical contribution to the $O(\alpha_s)$ result, they conspire to improve the stability of the cross section under changes of μ by a factor of 3–5, depending on the beam energy and PDF set (131). This stability and the agreement with data represent a remarkable success of perturbative QCD.

The charged-lepton rapidity asymmetry in W decays,

$$A(y) = \frac{d\sigma/dy(\ell^+) - d\sigma/dy(\ell^-)}{d\sigma/dy(\ell^+) + d\sigma/dy(\ell^-)}, \qquad 12.$$

Table 1 $\bar{p}p$ production cross sections times branching ratios for W and Z bosons. $\sigma_W \cdot BR$, $\sigma_Z \cdot BR$, and $R = \sigma_W \cdot BR/\sigma_Z \cdot BR$ at 630 and 1800 GeV[a]

	Data	Harriman et al (31)	MTE	MTB
$\sigma_W \cdot BR$ (pb) 630 GeV	UA1: 609 ± 41 ± 94 UA2: 682 ± 12 ± 40	733	699	720
$\sigma_Z \cdot BR$ (pb) 630 GeV	UA1: 58.6 ± 7.8 ± 8.4 UA2: 65.6 ± 4.0 ± 3.8	69.2	71.0	69.9
R (630 GeV)	UA1: $10.4^{+1.8}_{-1.5}$ ± 0.8 UA2: $10.4^{+0.7}_{-0.6}$ ± 0.3	10.6	9.9	10.3
$\sigma_W \cdot BR$ (nb) 1800 GeV	CDF: 2.20 ± 0.04 ± 0.20	2.06	2.02	2.10
$\sigma_Z \cdot BR$ (pb) 1800 GeV	CDF: 214 ± 11 ± 20	194	192	198
R (1800 GeV)	CDF: 10.0 ± 0.6 ± 0.4	10.6	10.5	10.6

[a] Data vs $O(\alpha_s^2)$ QCD for different PDF sets (131). BR($W \to \ell\nu_\ell$) = 0.109 and BR($Z \to \ell^+\ell^-$) = 3.35×10^{-2} PDF sets used are HMRSB (31) and Morfin & Tung sets E and B (33). First error in the data column is statistical, second error systematical.

is more sensitive to the choice of PDF set and is not affected by luminosity uncertainties. Its measurement probes directly the quark components and the sea flavor symmetry of the proton (133), necessary ingredients for a precise measurement of the W mass. Current data at $|y| < 2$ already discriminate between different PDF fits (135). The $O(\alpha_s)$ calculation of this asymmetry is available (136), and we hope that new data will extend the measurement to more forward regions, where the difference between PDFs is expected to be even more pronounced.

NLO calculations were also recently completed for the inclusive W and Z p_t distributions (137). Measurements have been reported by UA1, UA2, and CDF and are shown in Figure 20 (138, 139). The main source of systematic uncertainties in the p_t^W measurement is the determination of the neutrino transverse momentum, degraded by the energy resolution for the jets possibly present in the event. The small statistics (10% relative to the W) instead limit the otherwise very clean p_t^Z measurement.

The agreement with QCD is good at large p_t, which indicates consistency with the Standard Model expectations. At smaller p_t the theory is in better agreement with the UA2 data than with CDF. The small-p_t region is interesting from the theoretical point of view because a correct description of the spectrum requires the resummation of multiple gluon emission, which can be calculated in perturbative QCD (140) in the form of Sudakov form factors (12). These effects have been included in the theoretical curves shown here (141) using the techniques developed by Altarelli et al (142). Additional higher statistics measurements of the Z p_t spectrum will help turn the qualitative agreement indicated here into solid QCD tests in the delicate semi-inclusive $p_t \rightarrow 0$ region.

5.2 *Associated Jet Production*

The production of jets associated with W's and Z's is less well predicted than the inclusive momentum spectra. Nonetheless, the characteristics of multijet final states in these events are very topical since they form a background to top production. As with purely hadronic final states, most predictions for multijet characteristics in W and Z events are available only at tree level (146); hence absolute cross-section estimates have large uncertainties associated with the α_s^N terms. Recent work has led to new NLO predictions for quantities such as the jet E_t and the pseudorapidity distributions in W + 1 jet events (24).

CDF and UA1 measured the multiplicities of jets associated with W and/or Z production and compared the results to tree-level predictions (143, 144). Within the relatively large statistical and theoretical

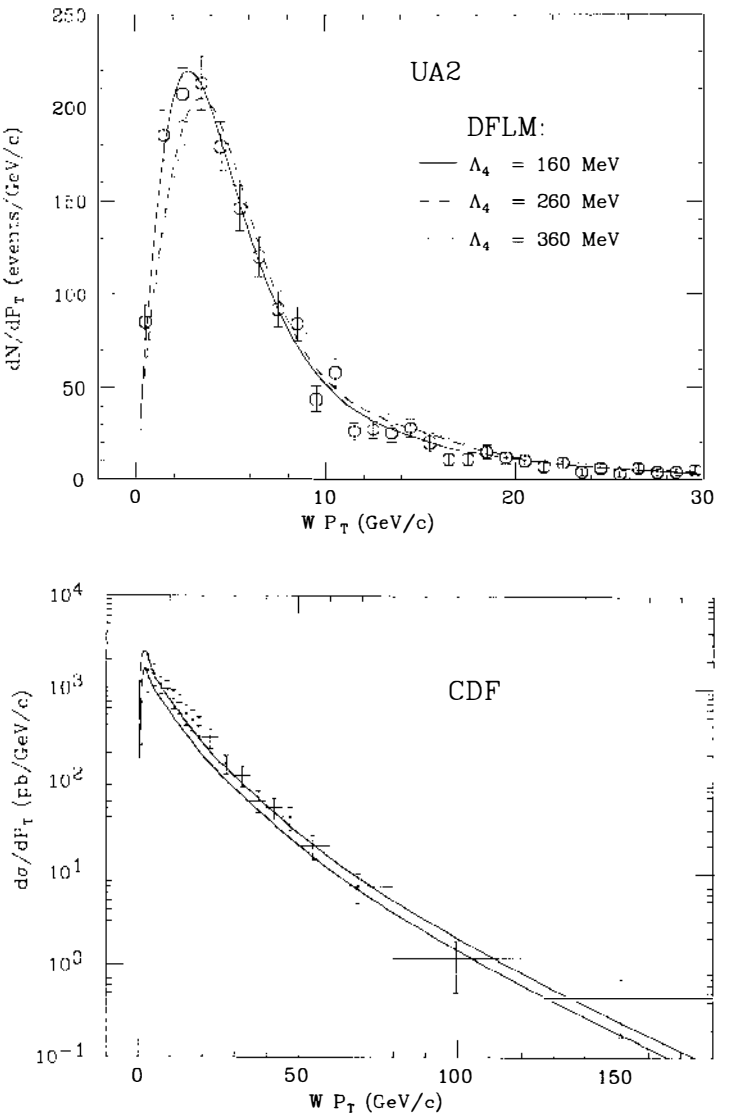

Figure 20 W p_t distribution at UA2 *(above)* and CDF *(below):* data versus QCD (141). The band indicates the theoretical uncertainty due to the choice of factorization scale and PDF sets.

uncertainties, the results are in good agreement with the theory. Figure 21 shows the cross section for W production as a function of jet multiplicity from CDF data. Other distributions, such as the E_t distribution of associated jets, show some discrepancy with tree-level predictions (145). New NLO predictions may improve the agreement with the data (24). With more data from the Tevatron, it is expected that a more thorough test of W and Z plus jet production can be carried out.

Using the ratio of the W + 1 jet and W + 0 jet event rates, and comparing it with the results of a leading order calculation for W + 1 jet production, UA2 (147) has extracted a measurement of $\alpha_s(M_W^2)$: $\alpha_s = 0.123 \pm 0.018\,(\text{stat.}) \pm 0.017\,(\text{syst.})$. This value is consistent with other determinations of α_s from LEP and DIS data (117). We point out that a fully consistent measurement of α_s and an extraction of Λ_{QCD} can, however, only be performed using a NLO calculation for the W + 1 jet process. Only at this order is it possible to reduce the μ scale uncertainties and to define a precise renormalization scheme within which α_s is measured. New analyses using the calculations of Giele et al (24) will follow, one hopes.

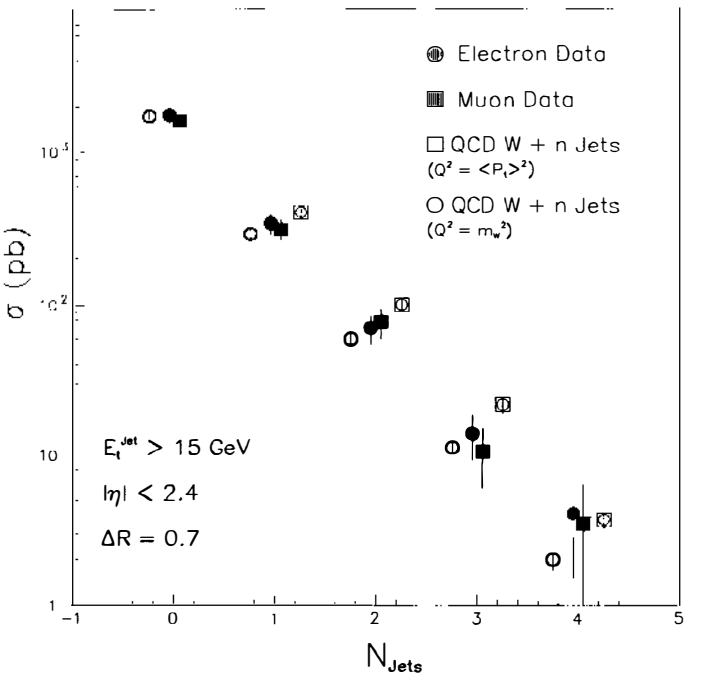

Figure 21 W + *n* jet production rates at $\sqrt{s} = 1.8$ TeV (143).

6 DIRECT PHOTONS

6.1 *Single-Photon Production*

As in the case of Drell-Yan events, the measurement of photons produced directly in a hadronic collision (148) has the advantage of not suffering from final-state strong interactions. Furthermore, since electromagnetic energy is detected with much better resolution than hadronic energy, systematic errors in the measurement of the photon momentum and direction are smaller than in jet measurements. Production of direct photons at small p_t is dominated by processes with a qg pair in the initial state, be they of the Compton or of the bremsstrahlung type (Figure 22). The capability of the experiments to observe direct photons at small p_t therefore provides yet another potential tool, in addition to the b quark measurements, for exploring the gluon content of the proton at small values of x, or alternatively for learning more about small-x phenomena. The associated production of photons and charm quarks has also been suggested as a direct probe of the charm density in the proton (149).

Several difficulties complicate the study of direct photons. First, there are severe backgrounds coming from hadrons such as π^0 and η's decaying into almost collinear photon pairs, mimicking a single γ. This background is statistically subtracted using two techniques. One technique relies on the differing probabilities that one photon or a photon pair will convert in a e^+e^- pair, the probability being independent of p_t. This "conversion method" can be used for arbitrarily large values of p_t. The second technique relies on the measurement of the transverse shape of the electromagnetic shower in the calorimeter to determine the fraction of events with two overlapping photons. This "profile method" can only be applied over a limited p_t range, above which the two photons are too close to be separated.

On the theoretical side, predictions depend on the knowledge of the bremsstrahlung contribution, which has both a perturbative and a nonperturbative piece. The latter is needed to define properly the boundary

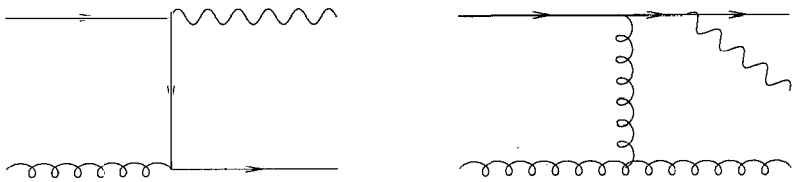

Figure 22 Sample diagrams contributing to prompt photon production. *Left:* leading order Compton scattering. *Right:* next-to-leading order bremsstrahlung.

condition of the perturbative parton → photon fragmentation function. It arises from the intrinsic hadronic component of the photon and it leads to a nonnegligible g → γ fragmentation probability via vector meson dominance (VMD).

To reduce the hadron decay backgrounds, experiments measure not a fully inclusive spectrum, but instead the so-called isolated photon spectrum. Isolation is defined in different ways. UA2 requires no charged tracks within a $\Delta\eta \times \Delta\phi = 0.2 \times 15°$ window around the γ direction, and no electromagnetic energy within $\Delta R < 0.265$. CDF requires the presence of less than 2 GeV of hadronic energy inside a cone of radius $\Delta R < 0.7$ surrounding the photon. The isolation reduces the bremsstrahlung contribution and emphasizes the purely perturbative effects, allowing for a more direct test of QCD (153–155).

Full NLO calculations are available for the inclusive spectrum (152) and the isolated p_t spectrum (153, 157), as well as for the photon + jet processes (156). A detailed study of the effects of isolation was presented by Berger & Qui (154). The comparison between theory and data is shown in Figure 23, which includes both UA2 and CDF results. While the agreement for $p_t > 20$ GeV is rather good, a discrepancy is apparent at smaller p_t values. This is even more clear at the Fermilab energy. Several effects could be responsible for this problem. We briefly survey them here.

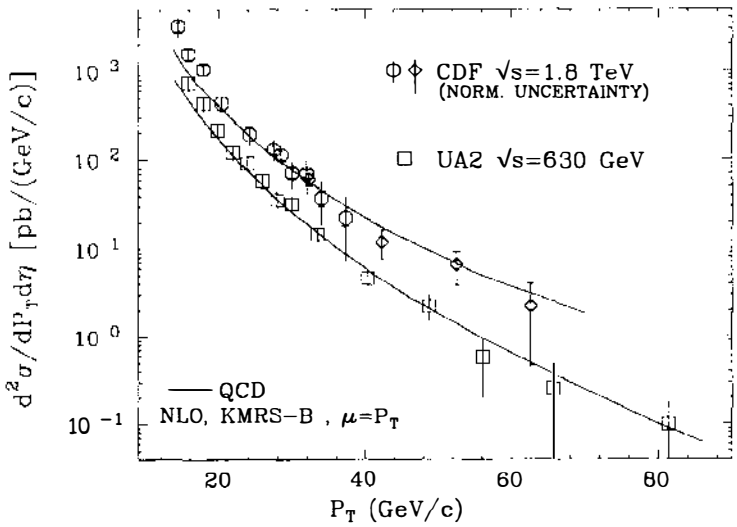

Figure 23 Isolated prompt photon p_t distribution at UA2 (150) and CDF (151), compared to a NLO QCD calculation (153). For CDF, profile *(circles)* and conversion *(diamonds)* methods have separate normalization uncertainties, shown in the legend.

First, as is always true in perturbation theory, there is an intrinsic scale uncertainty. Here the scales needed are three: for renormalization, initial-state factorization, and final-state fragmentation. Studies reported by Abe et al (151) indicate that the shape of the spectrum is rather insensitive to the scale uncertainty, at least in the p_t range probed experimentally. Not even the use of different PDF sets can accommodate the factor of two discrepancy observed for the lowest p_t bins (151). As in the b cross section (Figure 17), the values of p_t are probably too large to allow significant departures from current PDF fits.

The next possible effect is the bremsstrahlung contribution: how well do we know it? Aurenche et al (157) describe the full NLO correction to the bremsstrahlung processes, including a VMD description of the photon, as a phenomenological input for the evaluation of the $g \rightarrow \gamma$ fragmentation. The results indicate that higher order terms add at most 50% to the lowest order fragmentation contribution to the inclusive spectrum. After isolation cuts, their effect will be even smaller, because the $g \rightarrow$ isolated photon fragmentation is highly suppressed. We believe that 50% is therefore a reasonable estimate of the uncertainty reached today on the size of the bremsstrahlung contribution. Figure 24 shows

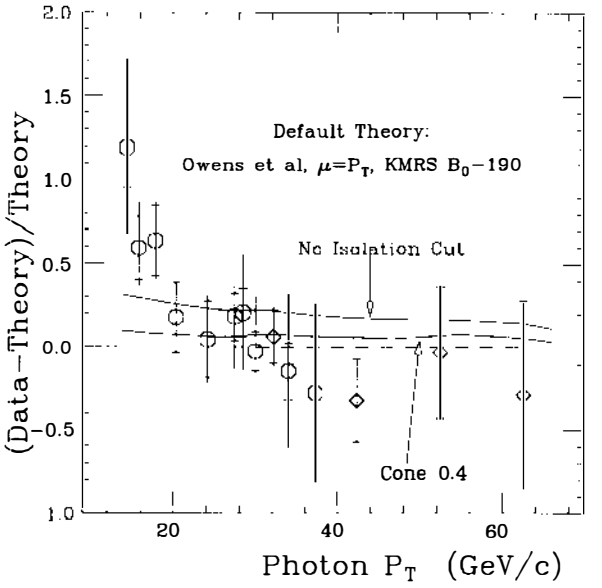

Figure 24 Study of the effect of isolation on the photon p_t spectrum at 1800 GeV (151). The solid lines indicate the relative variation of the theoretical calculation after reducing the isolation cone to 0.4, and after removing the isolation.

the effect of removing the isolation requirement from the NLO QCD calculation (151). This increases the QCD result by no more than 30%. A 50% uncertainty on this number is not sufficient to explain entirely the observed differences.

We cannot exclude the possibility that a combination of all three effects just considered, in addition perhaps to new data and a better understanding of the experimental systematics, can reestablish agreement between theory and observations. Another possibility is open, however: the violation of naive factorization at small x, as was discussed in Section 4. As in that case, new diagrams with a t-channel gluon exchange appear at next-to-leading order for the first time (Figure 22). The same considerations and techniques outlined previously apply to this case (109), even though no explicit calculation of the corrections to the differential p_t spectrum has been carried out as yet. This issue will have to be properly understood before the photon distributions—either in p_t or in rapidity—can be used to extract sensible measurements of the gluon structure functions in the small-x region (153, 158).

6.2 *Double-Photon Production*

Interesting measurements have also been performed on the direct production of photon pairs. Aside from its interest for QCD, this process is undergoing intense scrutiny as a possible dominant source of background to the detection of an intermediate mass Higgs boson at supercollider energies (159). The capability of QCD to estimate the $\gamma\gamma$ production rate accurately is therefore very important to establish.

Three processes contribute to the production of γ pairs (Figure 25): direct quark annihilation [$q\bar{q} \rightarrow \gamma\gamma$, $O(\alpha^2)$], gluon fusion via a quark box diagram [$gg \rightarrow \gamma\gamma$, $O(\alpha^2\alpha_s^2)$], and various bremsstrahlung contributions [$qg \rightarrow q\gamma\gamma$, $O(\alpha^2\alpha_s)$]. Even though of different order in α_s, these con-

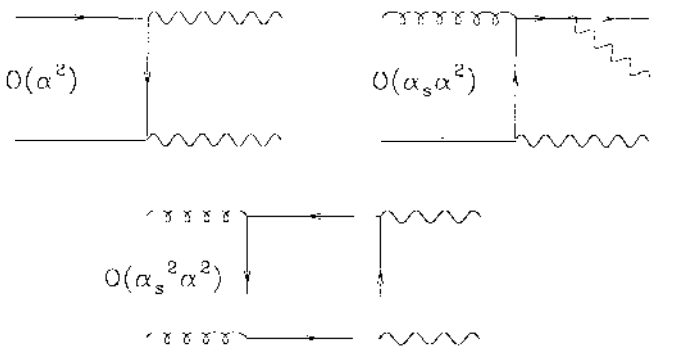

Figure 25 Sample diagrams contributing to double prompt photon production.

tributions are all comparable in magnitude over the currently measured p_t range, because at small x we have $q(x) \sim \alpha_s g(x)$. The complete $O(\alpha^2\alpha_s)$ calculation is available (161), including the effect of isolation cuts (162), together with the leading order $gg \rightarrow \gamma\gamma$ process. Data from UA2 (150) and CDF (160) are shown in Figure 26, compared to the relative calculations. In the UA2 data, the photons are not required to be isolated. Backgrounds and bremsstrahlung are reduced by applying the cut $\mathbf{p}_t(\gamma_1)\cdot\mathbf{p}_t(\gamma_2) < -0.7|\mathbf{p}_t(\gamma_1)|^2$. The theoretical calculations reproduce the experimental selection criteria.

The CDF data are systematically above the QCD curve, in particular at low p_t. UA2 shows a discrepancy only in the first p_t bin. In addition to the pure QCD curve, the figure shows the results obtained by the PYTHIA shower Monte Carlo, with and without the bremsstrahlung terms. The comparison between the different curves suggests that (*a*) PYTHIA has a bremsstrahlung contribution larger than NLO QCD, and (*b*) initial-state radiation induces a significant smearing of the p_t spectrum. It is perhaps premature to formulate a judgement on these measurements and the corresponding theory. On one side, the statistical errors are still large. On the other, the calculations have not been completed at the full $O(\alpha^2\alpha_s^2)$, where we know some important contributions ($gg \rightarrow \gamma\gamma$) but we ignore the effects of others a priori comparable in size, such as $gg \rightarrow q\bar{q}\gamma\gamma$. This last process would also contribute to a broadening of the $\gamma\gamma$ correlations with respect to the

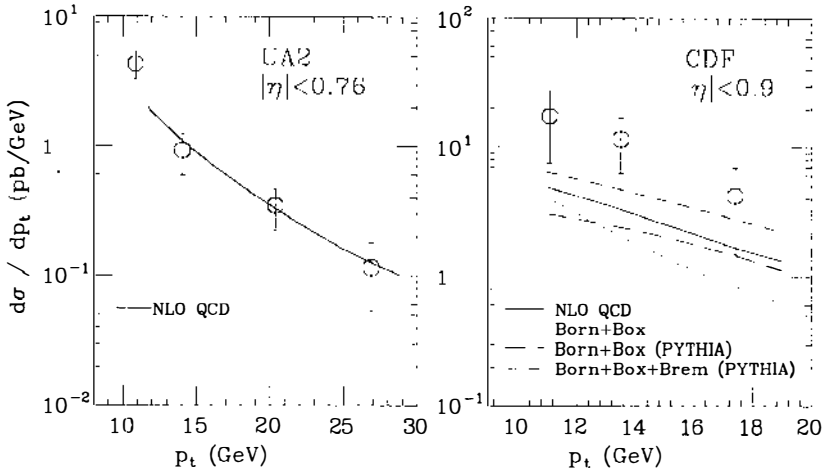

Figure 26 Double prompt photon p_t distribution at 630 GeV (150) and 1800 GeV (160), compared to predictions from next-to-leading order QCD (161, 162) and from the event generator PYTHIA (47). The p_t of both photons in each event enter in the plot.

available $O(\alpha^2\alpha_s)$ estimates, which are unable to explain the data (160). Last but not least, the values of x probed by this measurement are even smaller than those relevant for the b cross section; therefore this process is another interesting candidate for the study of small-x effects on production mechanisms.

CDF also measures the average transverse momentum of the photon pair, $\langle K_t \rangle = 5.1 \pm 1.1$ GeV. This value is consistent with that expected from perturbative initial-state radiation, $\langle K_t \rangle \sim \alpha_s \langle \sqrt{\hat{s}} \rangle \sim 4$ GeV, considering that the bremsstrahlung processes will contribute an additional unbalance. CDF quotes agreement with the prediction of the PYTHIA calculation for $\langle K_t \rangle$.

7. CONCLUSIONS

In order to describe the hard scattering processes in hadronic collisions properly, one needs some understanding of QCD. This argument is valid to the extent that the processes depend explicitly on α_s and on the parton distribution functions. Although QCD is widely accepted as the theory of strong interactions, progress can only result from making successively more rigorous tests, in which discrepancies are not idly dismissed, and both data and theoretical assumptions are closely examined.

In summarizing the status of QCD predictions, one can imagine two ways of classifying results. In the first, one could select phenomena according to the quality of the agreement between theory and experiment. In the second, one can select phenomena according to the presumed reliability of theoretical predictions and the corresponding faith in experimental results. It is a fact that processes believed to be reliably calculated also happen to belong to the class for which the agreement with data is good. This is the case for the one-jet inclusive distributions and for W and Z production, which should be considered as successes of the application of perturbative QCD to hadronic collisions. There is, however, a possible discrepancy in x_T scaling for jets, which should be an incisive test for the theory. As this article goes to print, there is no obvious explanation for such a discrepancy and we look forward to resolution, either from more data or from a new insight into the comparison with theory.

In contrast to inclusive jet and W,Z production, there are processes such as b quark and direct photon production in which the theoretical uncertainties are large even at next-to-leading order. Perturbative K factors are big and depend strongly on the choice of factorization and

renormalization scales. Even worse, the disagreement between theory and data seems to be larger than the presumed uncertainties can account for. With independent data for parton distributions in this range of x, it appears unlikely that one can find fault in a lack of knowledge of the gluon densities. There are, on the other hand, strong indications that a deeper understanding of the perturbative picture may be required to explain the discrepancies. For b cross sections, more data, particularly with the power of secondary vertex detectors, will provide strong checks on the existing data.

As indicated in the review of direct photon results, the processes contributing to photon or heavy quark production at next-to-leading order have singularities not present at tree level. For example, this is true in diagrams with a t-channel exchange. Since these singularities only appear at next-to-leading order, an even higher order calculation would be needed to have a true NLO approximation to all relevant processes. This does not represent a problem for the one-jet inclusive distributions nor for the W,Z and Drell-Yan events: in the first case, no new singularity appears at NLO (t-channel gluon exchange is already there at tree level); in the second case, the available calculations are already at NNLO. This distinction could explain why there appear to be two classes of processes.

Perturbative techniques for the study of multijet configurations are rapidly evolving, and the agreement with data is quite reasonable. These tests are crucial to the search for new phenomena in events containing multiple jets.

The measurement of finer details of the event structure, such as jet shapes, fragmentation, and multijet correlations, shows a good agreement with the results of both shower Monte Carlo and parton level calculations. This is therefore a success of perturbative QCD and of the way in which higher order processes are included in the Monte Carlo algorithms. These measurements support the concept of local parton-hadron duality and establish a firmer ground for the use of shower Monte Carlos to predict the fine details of the jet structure in hadronic collisions.

ACKNOWLEDGMENTS

We wish to thank the members of UA1, UA2, and CDF for making their results available for this review; in particular we thank D. Wood, P. Lubrano, and K. H. Meier. In the preparation of this review we benefited from discussions with S. Behrends, S. Ellis, R. K. Ellis, and Z. Kunszt.

Literature Cited

1. Gell-Mann M. *Acta Phys. Austriaca,* Suppl. IX: 733 (1972); Fritzsch H, Gell-Mann M, Leutwyler H. *Phys. Lett.* 47B:365 (1973); Weinberg S. *Phys. Rev.* D8:4482 (1973)
2. Gross DJ, Wilczek F. *Phys. Rev. Lett.* 30:1343 (1974); Politzer HD. *Phys. Rev. Lett.* 30:1346 (1974)
3. Altarelli G. *Annu. Rev. Nucl. Part. Sci.* 39:357 (1989)
4. Dokshitzer YuL, Dyakonov DI, Troyan SI. *Phys. Rep.* 58:270 (1980)
5. Mueller AH. *Phys. Rep.* 73:237 (1981)
6. Altarelli G. *Phys. Rep.* 81:1 (1982)
7. Wilczek F. *Annu. Rev. Nucl. Part. Sci.* 32:177 (1982)
8. Gribov LA, Levin EM, Ryskin MG. *Phys. Rep.* 100:1 (1983)
9. Bassetto A, Ciafaloni M, Marchesini G. *Phys. Rep.* 100:201 (1983)
10. Webber BR. *Annu. Rev. Nucl. Part. Sci.* 36:253 (1986)
11. Collins JC, Soper DE. *Annu. Rev. Nucl. Part. Sci.* 37:383 (1987)
12. Mueller AH, ed. *Perturbative QCD.* Singapore: World Scientific (1989), 614 pp.
13. Mangano ML, Parke SJ. *Phys. Rep.* 200:301 (1991)
14. Bethke S, Pilcher JE. *Annu. Rev. Nucl. Part. Sci.* 42:251 (1992); Hebbeker T. *Phys. Rep.* 217:69 (1992)
15. Eichten E, et al. *Rev. Mod. Phys.* 56: 579 (1984)
16. DiLella L. *Annu. Rev. Nucl. Part. Sci.* 35:107 (1985)
17. Bagnaia P, Ellis SD. *Annu. Rev. Nucl. Part. Sci.* 38:659 (1988)
18. Shapiro MD, Siegrist JL. *Annu. Rev. Nucl. Part. Sci.* 41:97 (1991)
19. Altarelli G, DiLella L, eds. *Proton-Antiproton Collider Physics.* Singapore: World Scientific (1989)
20. Barger V, Phillips RJN. *Collider Physics.* Reading, Mass: Addison-Wesley (1987)
21. Mishra SR, Sciulli F. *Annu. Rev. Nucl. Part. Sci.* 39:259 (1989)
22. Tung WK, Owens JF. *Annu. Rev. Nucl. Part. Sci.* 42:291 (1992)
23. Altarelli G, Parisi G. *Nucl. Phys.* B126:641 (1977); Dokshitzer YuL. *Sov. Phys. JETP* 46:641 (1977); Gribov VN, Lipatov LN. *Sov. J. Nucl. Phys.* 15:438 (1972)
24. Giele WT, Glover EWN, Kosower DA. *FERMILAB-PUB-92-230-T* (1992); Giele WT, Glover EWN. *Phys. Rev.* D46:1980 (1992)
25. Bern Z et al. *Phys. Lett.* B302:299 (1993); *Phys. Rev.* D38: 1888 (1988); Bern Z, Dixon L, Kosower DA. *SLAC-PUB-6001* (1992)
26. Diemoz M, et al. *Z. Phys.* C39:21 (1988)
27. Martin A, Roberts R, Stirling JW. *Phys. Rev.* D37:1161 (1988)
28. Aurenche P, et al. *Phys. Rev.* D39: 3275 (1989)
29. Glück M, Reya E, Vogt A. *Z. Phys.* C48:471 (1990)
30. Owens J. *Phys. Lett.* 266B:126 (1991)
31. Harriman P, et al. *Phys. Rev.* D42: 798 (1990)
32. Kwiecinski J, et al. *Phys. Rev.* D42: 3645 (1990)
33. Morfin J, Tung W. *Z. Phys.* C52:13 (1991)
34. Martin, et al. *Phys. Rev.* D47:867 (1993)
35. Botts J, et al. *Phys. Lett.* B304:159 (1993)
36. Amaudruz P, et al. *Phys. Lett.* B295: 159 (1992)
37. Mishra SR, et al. (CCFR). *Nevis Rep. NEVIS-1466* (1992); *Z. Phys.* C53:51 (1992)
38. Andersson B, Gustafson G, Sjöstrand T. *Z. Phys.* C6:235 (1980); *Nucl. Phys.* B197:45 (1982)
39. Webber B. *Nucl. Phys.* B238:492 (1984)
40. Azimov YI, et al. *Z. Phys.* C27:65 (1985); Dokshitzer YuL, Khoze VA, Troyan SI. See Ref. 12, p. 241
41. Amati D, Veneziano G. *Phys. Lett.* 83B:87 (1979); Marchesini G, Trentadue L, Veneziano G. *Nucl. Phys.* B181:335 (1981)
42. Odorico R. *Comp. Phys. Comm.* 32: 139 (1984)
43. Marchesini G, Webber BR. *Nucl. Phys.* B238:1 (1984)
44. Bengtsson HU, Ingelman G. *Comp. Phys. Comm.* 34:251 (1985)
45. Paige F, Protopopescu SD. *Brookhaven Rep. BNL-38034* (1986)
46. Field RD. *Nucl. Phys.* B264:687 (1986)
47. Sjöstrand T, Bengtsson M. *Comp. Phys. Comm.* 43:367 (1987)
48. Marchesini G, Webber B. *Nucl. Phys.* B310:461 (1988)
49. Catani S, Marchesini G, Webber BR. *Nucl. Phys.* B349:635 (1991)
50. Combridge BL, Kripfganz J, Ranft J. *Phys. Lett.* 70B:234 (1977); Owens JF, Reya F, Glück M. *Phys. Rev.*

D17:2324 (1978); *Phys. Rev.* D18: 1501 (1978)
51. Appel J, et al (UA2). *Phys. Lett.* 160B:349 (1985); Alitti J, et al (UA2). *Phys. Lett.* 257B:232 (1991)
52. Arnison G, et al (UA1). *Phys. Lett.* 172B:461 (1986)
53. Åkesson T, et al (AFS). *Phys. Lett.* 123B:133 (1983)
54. Abe F, et al (CDF). *Phys. Rev. Lett.* 62:613 (1989)
55. Ellis RK, et al. *Nucl. Phys.* B173:397 (1980)
56. Ellis RK, Sexton J. *Nucl. Phys.* B269:445 (1986)
57. Sterman G, Weinberg S. *Phys. Rev. Lett.* 39:1436 (1977); Furman M. *Nucl. Phys.* B197:413 (1982)
58. Aversa F, et al. *Phys. Lett.* 210B:225 (1988)
59. Ellis S, Kunszt Z, Soper D. *Phys. Rev. Lett.* 62:2188 (1989); 64:2121 (1990)
60. Ellis S, Kunszt Z, Soper D. *Phys. Rev. Lett.* 69:1496 (1992)
61. Arnison G, et al (UA1). *Phys. Lett.* 132B:214 (1983)
62. Beer A, et al. *Nucl. Instrum. Methods* 224:360 (1984); Appel J, et al. *Z. Phys.* C30:341 (1986)
63. Abe F, et al (CDF). *Phys. Rev.* D45: 1448 (1992)
64. Huth J, et al. In *Proc. 1990 Summer Study on High Energy Physics*, ed. E Berger. Singapore: World Scientific (1992), p. 134
65. Abe F, et al (CDF). *Phys. Rev. Lett.* 68:1104 (1992)
66. Abe F, et al. *Phys. Rev. Lett.* 70:713 (1993) (1992)
67. Ellis S, Kunszt Z, Soper D. *Phys. Rev. Lett.* 69:3615 (1992)
68. Aversa F, et al. *Z. Phys.* C49:459 (1991)
69. Bartel W, et al (JADE). *Z. Phys.* C33: 23 (1986)
70. Catani S, et al. *Phys. Lett.* 269B:432 (1991); Brown N, Stirling WJ. *Phys. Lett.* 252B:657 (1990), *Z. Phys.* C53: 629 (1992); Bethke S, et al. *Nucl. Phys.* B370:310 (1992)
71. Catani S, Dokshitzer YuL, Webber BR. *Phys. Lett.* 285B:291 (1992)
72. Abe F, et al. *Phys. Rev. Lett.* 70:1376 (1993) (1992)
73. Lane K, Ramana M. *Phys. Rev.* D44: 2678 (1991)
74. Frampton P, Glashow S. *Phys. Lett.* 190B:157 (1987)
75. Abe F, et al. *Phys. Rev.* D. In press
76. Abe F, et al (CDF). *Phys. Rev. Lett.* 69:2896 (1992)
77. Eichten E, et al. *Phys. Rev. Lett.* 50: 811 (1983)
78. Bagnaia P, et al (UA2). *Phys. Lett.* 144B:291 (1984); Arnison G, et al (UA1). *Nucl. Phys.* B276:253 (1986)
79. Abe F, et al (CDF). *Phys. Rev. Lett.* 65:968 (1990)
80. Althoff M et al (TASSO). *Z. Phys.* C22:307 (1984)
81. Paver N, Treleani D. *Z. Phys.* C28: 187 (1985); Humpert B, Odorico R. *Phys. Lett.* 154B:211 (1985); Landshoff PV, Polkinghorne JC. *Phys. Rev.* D18:3344 (1978)
82. Kunszt Z, Stirling W. *Phys. Lett.* 171B:307 (1986)
83. Berends F, Giele WT, Kuijf H. *Nucl. Phys.* B333:120 (1990); *Phys. Lett.* 232B:266 (1990)
84. Halzen F, Hoyer P. *Phys. Lett.* 130B: 326 (1983); Combridge BL, Maxwell CJ. *Nucl. Phys.* B239:429 (1984)
85. Parke S, Taylor T. *Phys. Rev. Lett.* 56:2459 (1986)
86. Kunszt Z, Stirling W. *Phys. Rev.* D56:2439 (1988)
87. Maxwell CJ. *Phys. Lett.* 192B:190 (1987)
88. Maxwell CJ. *Nucl. Phys.* B316:321 (1989); Mangano ML, Parke SJ. *Phys. Rev.* D39:758 (1989); Maxwell CJ, Parke SJ. *Phys. Rev.* D44:2727 (1991)
89. Alitti J, et al (UA2). *Phys. Lett.* 268B: 145 (1991)
90. Abe F, et al (CDF). *Fermilab Preprint* FERMILAB-PUB-93/003-E (1993), submitted to *Phys. Rev. Lett.*
91. Åkesson T, et al (AFS). *Z. Phys.* C34: 163 (1987)
92. Sjöstrand T, Sijl M. *Phys. Rev.* D36: 2019 (1987)
93. Abe F, et al (CDF). *Phys. Rev.* D45: 2249 (1992)
94. Duke DW, Owens JF. *Phys. Rev.* D30:49 (1984)
95. Meschi E (CDF). Presented at *DPF Meet. Am. Phys. Soc., Batavia, FNAL-CONF-92/340-E* (1992), to appear in the proceedings
96. Nir Y, Quinn HR. *Annu. Rev. Nucl. Part. Sci.* 42:211 (1992)
97. Nason P. In *Heavy Flavours*, Adv. Ser. on Directions in High Energy Physics, ed. M Lindner, AJ Buras. Singapore: World Scientific. In press
98. Ellis N, Kernan A. *Phys. Rep.* 195: 23 (1990)
99. Nason P, Dawson S, Ellis RK. *Nucl. Phys.* B303:607 (1988); Beenakker W, et al. *Phys. Rev.* D40:54 (1989)
100. Nason P, Dawson S, Ellis RK. *Nucl.*

Phys. B327:49 (1988); Beenakker W, et al. *Nucl. Phys.* B351:507 (1991)
101. Mangano M, Nason P, Ridolfi G. *Nucl. Phys.* B373:295 (1992)
102. Furmanski W, Petronzio R, Pokorski S. *Nucl. Phys.* B155:253 (1979); Mueller AH, Nason P. *Nucl. Phys.* B266:265 (1986); Mangano M, Nason P. *Phys. Lett.* 285B:160 (1992)
103. Azimov YaI, Dokshitzer YuL, Khoze VA. *Sov. J. Nucl. Phys.* 36: 878 (1982)
104. Peterson C, et al. *Phys. Rev.* D27:105 (83); Chrin J. *Z. Phys.* C36:163 (1987)
105. Colangelo G, Nason P. *Phys. Lett.* 285B:167 (1992)
106. Mele B, Nason P. *Nucl. Phys.* B361: 626 (1991)
107. Kunszt Z, Pietarinen E. *Nucl. Phys.* B164:45 (1980)
108. Lipatov LN, Frolov GV. *Sov. J. Nucl. Phys.* 13:333 (1971); Kuraev EA, Lipatov LN, Fadin VS. *Sov. Phys. JETP* 44:443 (1976); 45:199 (1977); Balitskii YaYa, Lipatov LN. *Sov. J. Nucl. Phys.* 28:822 (1978); Gribov LV, Levin EM, Ryskin MG. *Phys. Rep.* 100:1 (1983); Lipatov LN. See Ref. 12, p. 411
109. Ellis RK, Ross DA. *Nucl. Phys.* B345:79 (1990); Collins JC, Ellis RK. *Nucl. Phys.* B360:3 (1991)
110. Catani S, Ciafaloni M, Hautmann F. *Nucl. Phys.* B366:135 (1991)
111. Levin EM, Ryskin MG, Shabelsky YuM. *Phys. Lett.* 260B:429 (1991)
112. Albajar C, et al (UA1). *Phys. Lett.* 213B:405 (1988); 256B:121 (1991)
113. Albajar C, et al (UA1). *Phys. Lett.* 273B:540 (1991)
114. Abe F, et al (CDF). *Phys. Rev. Lett.* 68:3403 (1992)
115. Vejcik S (CDF). See Ref. 95
116. Huffman BT (CDF). See Ref. 95; *FNAL-CONF-92/337-E*
117. Bethke S. In *Perturbative QCD and Hadronic Interactions,* ed. J Tran Thanh Van, p. 203. Editions Frontieres: (1992); Altarelli G, presented at *QCD 20 years later,* Aachen, CERN-TH. 6623/92 (1992)
118. Berger EL, Meng R, Qiu J. *Proc. 26th Int. Conf. on HEP, Aug 6–12, 1992, Dallas.* In press
119. Mangano M. *Z. Phys.* C. In press
120. Geiser A. See Ref. 117, p. 159
121. Guberina G, et al. *Nucl. Phys.* B174: 317 (1980); Berger EL, Jones D. *Phys. Rev.* D23:1521 (1981); Baier R, Rückl R. *Z. Phys.* C19:251 (1983); Humpert B. *Phys. Lett.* 184B:105 (1987); Gastmans R, Troost W, Wu TT. *Nucl. Phys.* B291:731 (1987)
122. Glover EWN, Martin AD, Stirling WJ. *Z. Phys.* C38:473 (1988); Glover EWN, Halzen F, Martin AD. *Phys. Lett.* 185B:441 (1987)
123. Albajar C, et al (UA1). *Phys. Lett.* 200B:380 (1988); 256B:112 (1991)
124. Abe F, et al. *Phys. Rev. Lett.* 69:3704 (1992)
125. Boswell C (CDF). See Ref. 95, *FNAL-CONF-92/347-E* (1992)
126. Deleted in proof
127. Braaten E, Yuan TC. *NUHEP-TH-92-23; UCD-92-25* (1992)
128. Poling RA. In *Joint Int. Symp. and Europhysics Conf. on High Energy Physics,* ed. S Hegarty et al. Singapore: World Scientific (1992), p. 546
129. Albajar C, et al (UA1). *Phys. Lett.* 253B:503 (1991); Alitti J, et al (UA2). *Phys. Lett.* 276B:365 (1992)
130. Abe F, et al (CDF). *Phys. Rev.* D44: 29 (1991); *Phys. Rev. Lett.* 69:28 (1992)
131. Hamberg R, Matsuura T, van Neerven WL. *Nucl. Phys.* B359:343 (1991); van Neerven WL, Zijlstra EB. *Nucl. Phys.* B382:11 (1992)
132. Sterman G. *Nucl. Phys.* B310:281 (1987); Catani S, Trentadue L. *Nucl. Phys.* B327:323 (1989)
133. Halzen F. In *Proc. Hadron Structure Functions and Parton Distributions,* ed. DF Geesaman et al. Singapore: World Scientific (1990); Berger EL, et al. *Phys. Rev.* D40:83 (1989); Erratum, *Phys. Rev.* D40:3789 (1989)
134. Deleted in proof
135. Abe F, et al (CDF). *Phys. Rev. Lett.* 68:1458 (1992)
136. Baer H, Reno MH. *Phys. Rev.* D43: 2892 (1991)
137. Arnold PB, Reno MH. *Nucl. Phys.* B319:37 (1989); Gonsalves RJ, Pawlowski J, Wai CF. *Phys. Rev.* D40: 2245 (1989)
138. Albajar C, et al (UA1). *Z. Phys.* C44: 15 (1989); Alitti J, et al (UA2). *Z. Phys.* C47:523 (1990)
139. Abe F, et al (CDF). *Phys. Rev. Lett.* 66:2951 (1991); 67:2937 (1991)
140. Dokshitzer YuL, Dyakonov DL, Troyan SI. *Phys. Lett.* 78B:290 (1978); Parisi G, Petronzio R. *Nucl. Phys.* B154:427 (1979); Kodaira J, Trentadue L. *Phys. Lett.* 112B:66 (1982)
141. Arnold PB, Kaufmann RP. *Nucl. Phys.* B349:381 (1991)
142. Altarelli G, et al. *Nucl. Phys.* B246: 12 (1984); *Z. Phys.* C27:617 (1985)
143. Rodrigo T (CDF). See Ref. 95, *FNAL-CONF-92/342-E* (1992), to appear in the proceedings

144. Albajar C, et al (UA1). *Z. Phys.* C44: 15 (1989)
145. Huth J (CDF). *FERMILAB-CONF-92/326-E* (1992); In *Proc. 26th Int. Conf. on HEP, Aug. 6–12, 1992, Dallas.* In press
146. Gunion J, Kunszt Z. *Phys. Lett.* 161B:333 (1985); Kleiss R, Stirling WJ. *Nucl. Phys.* B262:235 (1985); Hagiwara K, Zeppenfeld D. *Nucl. Phys.* B313:560 (1989); Berends FA, Giele WT, Kuijf H. *Nucl. Phys.* B321:39 (1989); Berends FA, et al. *Nucl. Phys.* B357:32 (1991)
147. Alitti J, et al (UA2). *Phys. Lett.* 263B: 563 (1991)
148. Berger EL, Braaten E, Field RD. *Nucl. Phys.* B239:52 (1984); Ferbel T, Molzon WR. *Rev. Mod. Phys.* 56:181 (1984); Owens J. *Rev. Mod. Phys.* 59: 465 (1987)
149. Fletcher RS, Halzen F, Zas E. *Phys. Lett.* 221B:403 (1989)
150. Albajar C, et al (UA1). *Phys. Lett.* 209B:385 (1988); Alitti J, et al (UA2). *Phys. Lett.* 288B:386 (1992)
151. Abe F, et al (CDF). *Phys. Rev. Lett.* 68:2734 (1992); *FERMILAB-PUB-92/01-E* (1992)
152. Aurenche P, et al. *Phys. Lett.* 140B: 87 (1983); *Nucl. Phys.* B286:509 (1987); B297:661 (1988)
153. Aurenche P, Baier R, Fontannaz M. *Phys. Rev.* D42:1440 (1990)
154. Berger EL, Qiu J. *Phys. Rev.* D44: 2002 (1991)
155. Kunszt Z, Trocsanyi Z. *ETH-TH/92-26* (1992); Glover EWN, Stirling WJ. *Phys. Lett.* 295B: 128 (1992)
156. Baer H, Ohnemus J, Owens JF. *Phys. Rev.* D42:61 (1990)
157. Aurenche P, et al. *LPTHE-Orsay 92/30, ENSLAPP-A-386/92* (1992)
158. Alitti J, et al. *Phys. Lett.* B299:174 (1993)
159. Seez C, et al. In *Proc. LHC Workshop Aachen,* ed. G Jarlskog D Rein, *CERN 90-10,* (1990), 2:474
160. Abe F, et al. *Phys. Rev. Lett.* 70:2232 (1993)
161. Aurenche P, et al. *Z. Phys.* C29:459 (1985)
162. Bailey B, et al. *Phys. Rev.* D46:2018 (1992)